Sedimentary Geology 445 (2023) 106327

Contents lists available at ScienceDirect

Sedimentary Geology

journal homepage: www.elsevier.com/locate/sedgeo

Seismically-induced down-sagging structures in tephra layers (tephra-seismites) preserved in lakes since 17.5 cal ka, Hamilton lowlands, New Zealand

Max O. Kluger [a,*], David J. Lowe [a], Vicki G. Moon [a], Jordanka Chaneva [a], Richard Johnston [b], Pilar Villamor [c], Tehnuka Ilanko [a], Richard A. Melchert [a], Rolando P. Orense [d], Remedy C. Loame [a], Nic Ross [e]

[a] School of Science/Te Aka Mātuatua, University of Waikato, Hamilton, New Zealand
[b] Faculty of Science and Engineering, Swansea University, Swansea, United Kingdom
[c] GNS Science, Lower Hutt, New Zealand
[d] Department of Civil and Environmental Engineering, University of Auckland, Auckland, New Zealand
[e] Hamilton Radiology, Hamilton, New Zealand

ARTICLE INFO

Article history:
Received 12 November 2022
Received in revised form 23 December 2022
Accepted 27 December 2022
Available online 5 January 2023

Editor: Dr. Catherine Chagué

Keywords:
Soft-sediment deformation structures (SSDSs)
Tephra
Liquefaction
Palaeoearthquakes
Kerepehi Fault
Te Puninga Fault

ABSTRACT

We analysed numerous soft-sediment deformation structures (SSDSs) identified in seven unconsolidated, up to 8-cm thick, siliceous tephra layers that had been deposited in ~35 riverine-phytogenic lakes within the Hamilton lowlands, northern North Island, New Zealand, since 17.5 calendar (cal) ka BP. Based on sediment/tephra descriptions and X-ray computed tomography scanning of cores taken from ten lakes, we classified these SSDSs into elongated load structures (i.e., down-sagging structures) of different dimensions, ranging from millimetre- to decimetre-scale, and centimetre-long dykes. Down-sagging structures were commonly manifested as intrusions of internal tephra beds of very fine to medium sand into underlying organic lake sediments. The tephra layers commonly exhibited an upper silt bed, which was not directly affected by deformation. Dry bulk density and grain size distribution analyses of both the organic lake sediment and the internal tephra beds provided evidence for the deformation mechanism of down-sagging structures and their driving force: the organic lake sediment and the upper silt bed are less liquefiable, whereas the very fine to medium sand internal tephra beds are liquefiable. The tephra layers and encapsulating organic lake sediments formed three-layer (a–b–a) density systems, where 'a' denotes the sediment unit of lower density. We infer that downward-directed deformation was favoured by the a–b–a density system with the upper, less-liquefiable, silt bed within the tephra layer preventing upward intrusion during the liquefaction process. The spatial distribution and ages of SSDSs within the lakes provided some evidence that liquefaction of the older tephra layers, i.e., Rerewhakaaitu, Rotorua, and Waiohau tephras, deposited 17.5, 15.6, and 14 cal ka BP, respectively, was triggered by a seismic source to the northeast of the Hamilton lowlands (i.e., Kerepehi and/or Te Puninga faults). In contrast, the liquefaction of the younger tephra layers, i.e., Opepe, Mamaku, and Tuhua tephras, deposited 10.0, 8.0, and 7.6 cal ka BP, respectively, may have been triggered by movement on local faults within the Hamilton lowlands, namely the Hamilton Basin faults, or by distant faulting at the Hikurangi subduction margin east of North Island.

1. Introduction

Soft-sediment deformation structures (SSDSs) occur in unconsolidated sediments during or shortly after their deposition, and before significant diagenesis (Owen et al., 2011). Common SSDSs include water-escape and injection structures, load structures, convolute laminations, deformed cross-bedding, slumps, and collapse structures (Obermeier, 1996; Rodríguez-Pascua et al., 2000; Kang et al., 2010; Owen and Moretti, 2011; Mazumder et al., 2016). Water-escape and injection structures are commonly formed when sediment is transported upwards by the expulsion of water during the process of fluidisation and liquefaction, resulting in dykes, sills, disk-and-pillar structures, and sand volcanoes (Owen et al., 2011). Liquefaction describes the loss of grain contacts and a temporary transfer of grain weight to the pore fluid under undrained conditions, and is seen as the most common mechanism for the formation of dykes (Nichols, 1995).

* Corresponding author.
E-mail address: max.kluger@waikato.ac.nz (M.O. Kluger).

https://doi.org/10.1016/j.sedgeo.2022.106327
0037-0738/

Downward-directed SSDSs occur either from mainly passive collapse of overlying materials into fissures and cracks, caused by extensional tectonics or glaciogenic processes (i.e., neptunian dykes) (Obermeier, 1996; Bektas et al., 2001; Montenat et al., 2007; Moretti and Sabato, 2007; Fortuin and Dabrio, 2008; Kang et al., 2010; El Taki and Pratt, 2012; Basilone et al., 2016; Lunina and Gladkov, 2016; Mazumder et al., 2016; Ozcelik, 2016; Gavrilov, 2017), or from liquefaction in reverse density gradient systems forming load structures (Anketell et al., 1970; Owen, 2003; Gladkov et al., 2016; Belzyt et al., 2021). Reverse density gradient systems are denoted as b–a density systems, where 'a' refers to the sediment unit of relatively lower density (Anketell et al., 1970). Load structures are common in two-layer b–a density systems, but have only been sparsely reported in three-layer a–b–a density systems, where a dense sediment is interlayered between members of relatively lower density (Moretti and Ronchi, 2011; Törő and Pratt, 2016).

To improve the understanding of sediment deformation processes in a–b–a density systems, a comprehensive multidisciplinary analysis was conducted on records of late Quaternary sediment cores taken from lakes, formed about 20 calendar (cal) ka, that lie in the Hamilton lowlands (northern New Zealand) amidst newly-discovered Hamilton Basin faults (Fig. 1) (Moon and de Lange, 2017). The cores comprise highly organic, unconsolidated lake sediments of low density with interlayered, silicic tephra-fall deposits (layers up to 8-cm thick) of relatively higher density, each of which forms an individual a–b–a density system with the enclosing lake sediment. Tephra deposits are the explosively-erupted, unconsolidated, pyroclastic products of a volcanic eruption of any grain size or composition (Lowe, 2011). Palaeoliquefaction in tephra deposits has been rarely investigated previously. Only a handful of papers on the topic is known to us (Sieh and Bursik, 1986; Mazumder et al., 2016; Yang et al., 2019; Brlek et al., 2020; Molenaar et al., 2021). Following the commonly accepted concept of liquefaction discussed above, sediment deformations in a–b–a density systems should be directed upwards, following the direction of least resistance. However, in our lake records, the tephra layers were almost exclusively deformed downwards, forming SSDSs in the form of several decimetre-long, elongated load structures (Fig. 2) (Lowe, 1988b).

The SSDSs were imaged using X-ray computed tomography (CT), described in cross-section, and then analysed via bulk density measurement, grain size distribution analyses, and determination of Atterberg limits. Then, their mechanisms of deformation, the driving force of deformation, and possible triggering mechanisms, were interpreted following the protocols provided by Owen and Moretti (2011). The spatial and temporal occurrence of SSDSs was mapped across the studied lakes within the Hamilton lowlands and an attempt was made to link the occurrence of the SSDSs to seismic activity on regional faults including two faults in the adjacent Hauraki Plains, the Kerepehi and (newly-identified) Te Puninga faults (Persaud et al., 2016; Van Dissen et al., 2021), as well as on the local faults within the Hamilton lowlands (the Hamilton Basin faults) (Van Dissen et al., 2021).

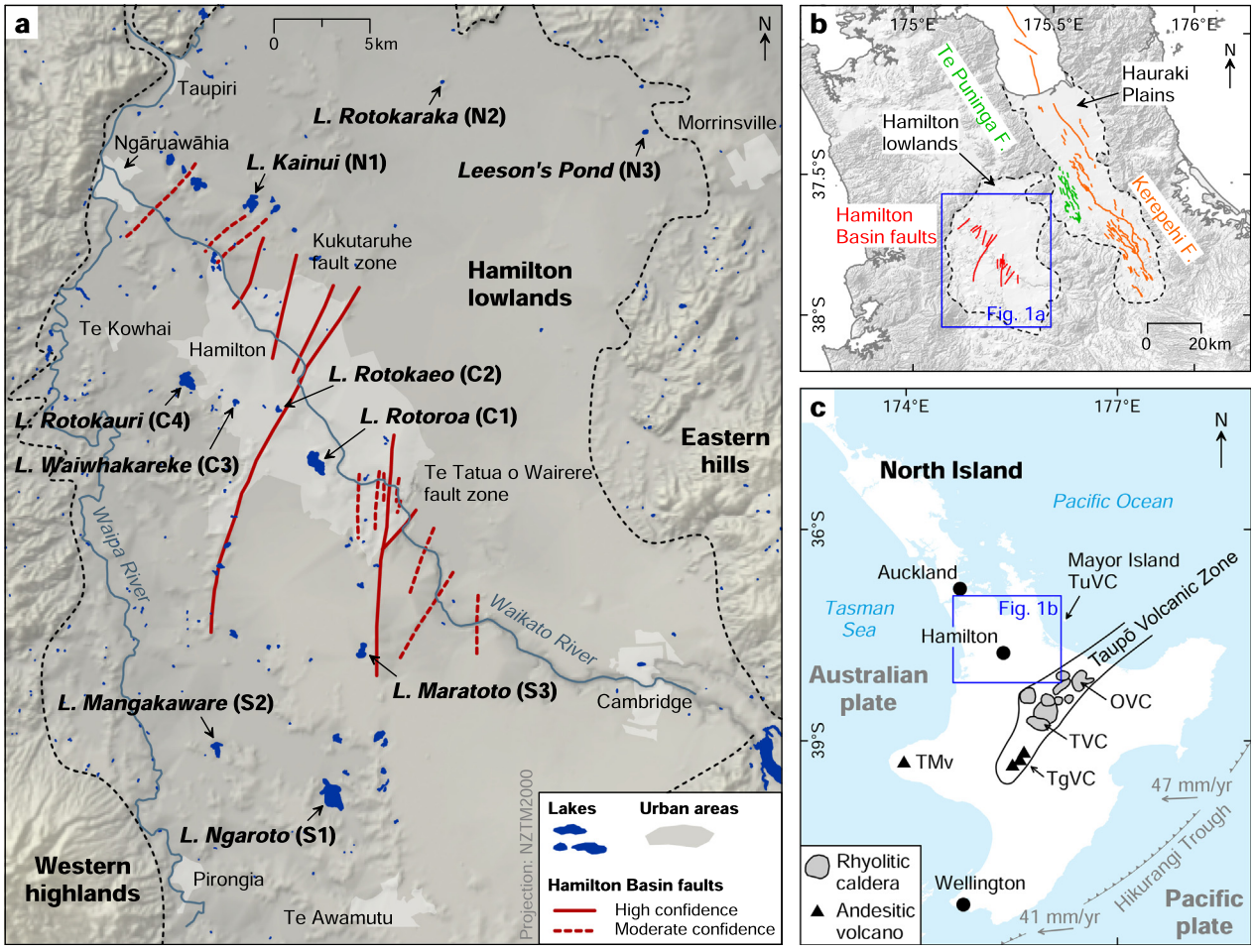

Fig. 1. Study area. (a) Locations of ten lakes cored in our study and recently identified faults (Moon and de Lange, 2017; Van Dissen et al., 2021) in the Hamilton lowlands (in the Hamilton Basin). Base map is a low-resolution DEM from Land Information New Zealand. *L.* = Lake. Abbreviated lake names are provided in parentheses. (b) Wider view of the locations of faults in the Hamilton Basin (a) and the Te Puninga and Kerepehi faults in adjacent Hauraki Plains (Persaud et al., 2016). (c) Map of the North Island, New Zealand, with general tectonic setting and the main volcanic centres active since 20 cal ka (Leonard et al., 2010). The tephra deposits preserved in the lakes originated from Okataina (OVC), Taupō (TVC), Tongariro (TgVC), and Tuhua (TuVC) volcanic centres, and Taranaki Maunga volcano (TMv).

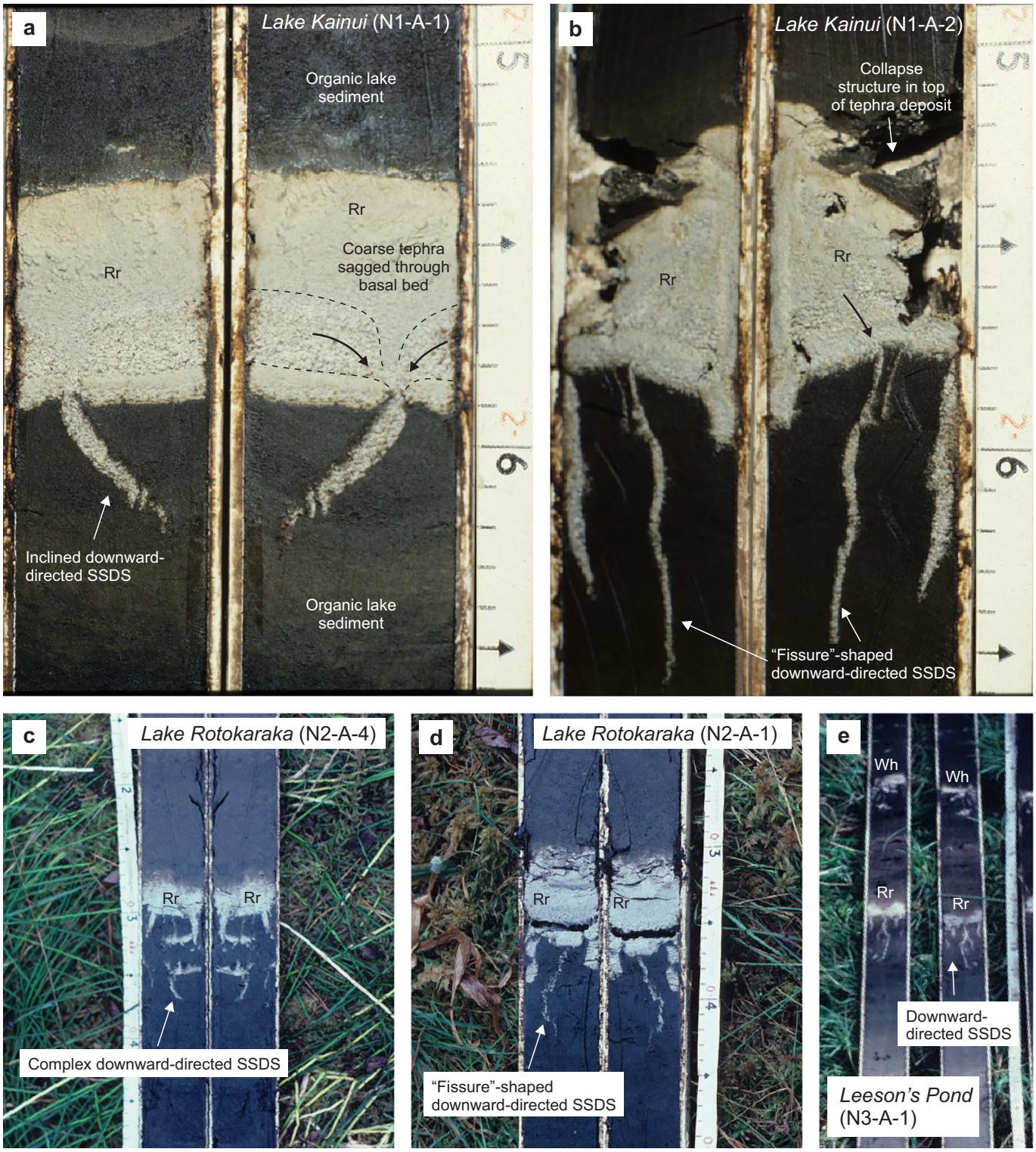

Fig. 2. Examples of downward-directed SSDSs in Rotorua (Rr) tephra layers in historic cores from various lakes (i.e., Kainui, Rotokaraka, Leeson's Pond). For locations of lakes see Fig. 1a. (a) Down-sagging structure with internal flow structures indicating pore pressure release (Lowe, 1988b). (b) Up to 20-cm long, fissure-like down-sagging structure (Lowe, 1988b). (c–e) Down-sagging structures. Wh = Waiohau tephra. The scale bars are in cm.

2. Geological setting

The Hamilton lowlands lie within the tectonically formed Hamilton Basin in the northern North Island of New Zealand (Fig. 1a–b), adjacent to tephra-generating volcanic centres in the Taupō Volcanic Zone, offshore Tuhua Volcanic Centre, and distant Taranaki Maunga volcano (Fig. 1c). The basin's most recent infilling deposits – Quaternary ignimbrites, volcanogenic alluvium, and tephra deposits – underlie low hills surrounded and partly buried by younger, secondary volcaniclastic alluvium, the Hinuera Formation, deposited ~20 cal ka by the ancestral Waikato River (Hume et al., 1975; Selby and Lowe, 1992; Manville and Wilson, 2004; Peti et al., 2021).

Around 35 riverine and riverine-phytogenic lakes occur adjacent to the antecedent hills. Deposition of the Hinuera Formation across the mouths of small valleys formed alluvial dams, generating shallow basins in which groundwater and drainage formed these blocked-valley riverine lakes (Green and Lowe, 1985; Lowe and Green, 1992; Lowe and Green, 2023). In many cases, massive peat growth on top of the alluvium formed a second-storey dam, resulting in larger, peat-dominated riverine-phytogenic lakes (Green and Lowe, 1985, 1994). These closed-basin lakes have provided a repository since ~20 cal ka for ~40 distal tephra deposits, as well as numerous cryptotephras, preserved in ~3–6 m of organic lake sediment (Lowe, 1988b; Loame et al., 2018). Derived from rhyolitic and andesitic eruptions in Taupō Volcanic Zone, Tuhua Volcanic Centre, and Taranaki Maunga volcano, these tephras range from sub-millimetre to ~8 cm in thickness, the thickest layers being rhyolitic (Lowe, 1988b, 2019).

SSDSs have already been recorded in some of the tephra layers (Lowe, 1988b) as elongated, sometimes fissure-like load structures with pointy ends, each load structure being up to a few centimetres wide and up to 20 cm long (Fig. 2). The load structures were commonly associated with prominent collapse structures at the top of the tephra layer (Fig. 2b), indicating volume loss of the tephra layer during downward-directed intrusion into underlying organic lake sediments. Lowe (1988b) suggested (with some uncertainty expressed) that bioturbation was the only plausible mechanism that could have caused the downward-directed SSDSs in the tephra layers because, at that time, the Hamilton lowlands were believed to lack active faults (Edbrooke, 2005; Langridge et al., 2016) and therefore designated as having low to moderate seismic risk (Stirling et al., 2012). However, new evidence of faults (Fig. 1) and seismic activity, including within the Hinuera Formation (Hume et al., 1975; Kleyburg et al., 2015; Persaud et al., 2016; Moon and de Lange, 2017; Van Dissen et al., 2021), now provide a seismogenic explanation for the downward-directed SSDSs.

3. Materials and methods

3.1. Coring

Ten lakes from three different parts in the Hamilton lowlands were cored: three in the south (Ngāroto, Mangakaware, Maratoto), four in the centre (Rotoroa, Rotokaeo, Waiwhakareke, Rotokauri), and three in the north (Kainui, Rotokaraka, Leeson's Pond) (Fig. 1a). The distance between the southernmost lake (Ngāroto) and the northernmost one (Rotokaraka) is ~40 km. For each lake, one or more cores ~1.5–2 m in length were collected from partly overlapping sediment depths using a modified Livingstone piston corer with a 50-mm internal diameter PVC coring tube (Rowley and Dahl, 1956) for historical cores taken in the 1980s, and 65- or 80-mm internal diameter for cores taken more recently in 2016, 2020, and 2022.

The cores in most cases were collected from the deepest basin(s) of the lakes where typically the thickest sediments occur, and where the tephra beds are essentially horizontal (Lowe, 1985) and unaffected by other aseismic trigger mechanisms specific to other depositional environments (Owen and Moretti, 2011). In Lake Maratoto, the cores were extracted from ten sites throughout the lake (Green and Lowe, 1985), whereas at Lake Rotoroa, seven sites throughout the lake were selected for coring including in shallow areas. Where more than one core was required to fully capture the entire sediment thickness in the lake, overlapping cores were taken and then easily correlated using the distinctive physical properties of the glass-rich tephra layers present in the lake sediments, the layers being typically different in colour and thickness (e.g., see illustrations in Green and Lowe, 1985; Lowe, 1988b, 2019), to generate a composite core ~3–5 m in length for each lake. An example showing the construction of a composite core using tephrochronology is provided in Supplementary Fig. S1.

In most lakes, duplicate cores were also collected from different sites within the lake basin. Because of the duplication and the overlapping cores, the majority of tephra layers could be investigated more than once in each lake (up to 20 times in Lake Maratoto; Green and Lowe, 1985), increasing the confidence in characterising SSDSs. The sediment strata and stratigraphy of all but two lakes (Waiwhakareke, Rotokaeo) have been described previously (Green and Lowe, 1985; Lowe, 1985, 1988b, 2019). Additional information about the sediment cores is provided in Supplementary Table S1.

3.2. CT imaging

X-ray computed tomography (CT) imaging was performed using a medical CT scanner on all whole-round cores prior to opening (except for historical cores from lakes Mangakaware, Maratoto, Rotokaraka, and Leeson's Pond, which were not available for CT imaging). CT volumes were processed using imageJ, Drishti ver. 2.7 (Limaye, 2012), VGStudio Max (ver. 2.1.5, Volume Graphics, Germany), and Syglass (ver. 1.6, IstoVisio, Inc. Morgantown, WV) (Pidhorskyi et al., 2018). Drishti and imageJ were used to create tiff slices from DICOM files. Slice data were loaded into Syglass, volumetric virtual reality software. The physical cuts through the core samples were correlated to the precise virtual slice within the 3D CT data using a co-registration tool within Syglass utilising four fiducial markers across the 3D X-ray volume and the 2D core cut image – a methodology previously demonstrated in 3D scanning electron microscope data to confocal microscopy images of brain tissue (Thomas et al., 2021).

Once the physical core cut was identified in the 3D X-ray CT volumes, the data were loaded into VGStudio Max and, to aid subsequent segmentation, the outer plastic tubing of the core was excluded using the ellipse selection tool to isolate the material inside the tube in the sagittal plane. The organic lake sediments above and below the tephra layers were removed digitally in both VGStudio and Syglass by applying a global histogram threshold based on X-ray attenuation, which was significantly different between the two constituents, and allowed images and videos to be exported revealing only the tephra deposit. The global histogram threshold was chosen to best correlate the tephra SSDSs (at a longitudinal slice through the centre of the X-ray CT volume) to the physical cut of the lake core.

3.3. Characterisation of tephra layers

Individual tephra layers in each core were classified into three types: (i) 'SSDS' (i.e., some kind of SSDS was identified), (ii) 'intact' (i.e., no post-depositional deformation of tephra layer was identified), or (iii) 'discontinuous' (i.e., the tephra layer exhibited some kind of disruption that could not be definitely associated with any SSDS), on the basis of detailed sediment description and CT imaging. Supplementary Fig. S2 shows typical examples of tephra layers classified as discontinuous because they were disrupted, varied in thickness within the extent of the core, were partly covered by sawdust from the core liner, or were located at the base of the core and, thus, could not be characterised satisfactorily. Discontinuous tephra layers were not considered further because of uncertainty about whether the disturbance was caused by liquefaction or by other processes.

The other tephra layers (classified as 'SSDS' or 'intact'), and the organic lake sediments, were further characterised by means of dry bulk density measurements, grain size distribution analyses, organic content, and Atterberg limits. Locations and depths of samples analysed by the four methods are provided in Supplementary Table S2. Bulk density was determined by cutting tephra layers and organic lake sediments into rectangular prisms of varying dimensions depending on the available volume. A cutter knife was used in order to cut prisms without causing too much disturbance to the soil structures of the samples. Volumes of bulk density samples varied from 1 to 40 cm^3. Dry bulk densities were determined multiple times to aid the reliable (reproducible) calculation of mean values with sufficient confidence: organic lake sediment (eight samples), Tuhua tephra (eleven samples), Mamaku tephra

(six samples), Waiohau tephra (six samples), and Rotorua tephra (16 samples). Grain size distribution analyses were performed using a Malvern Mastersizer 3000. Grain size distribution curves were processed using GRADISTAT 9.1 (Blott and Pye, 2001) and basic statistical parameters were determined using the geometric method of moments (Krumbein and Pettijohn, 1938). Grain size nomenclature is based on standard sedimentological class boundaries (Folk, 1980) with clay defined as particles <2 μm in diameter. Where applicable, equivalent classes based on volcanological grain size classes (White and Houghton, 2006) are provided. Atterberg limits and organic content were determined on representative organic lake sediments (ASTM D 4318-17e1, 2017; ASTM D7348-21, 2021).

The dimensions of SSDSs were analysed and compared to the total tephra thickness and the thickness of internal beds of tephra layers. For every instance where a tephra layer exhibited one or more SSDSs in a core, the area of all SSDSs associated with this particular tephra layer was measured using a geographic information system (GIS). The total area of SSDSs was then averaged by the number of SSDSs observed in the tephra layer. The area of SSDSs was considered here to represent a first level approximation of the volume of SSDSs. The dimensions of SSDSs were further quantified by measuring the maximal vertical length of the SSDSs.

4. Sedimentary facies

The sedimentary succession as present in sediment cores taken from the riverine and riverine-phytogenic lakes in the Hamilton lowlands comprised three main geological units, namely pre-lake volcanogenic alluvial deposits (Hinuera Formation), organic lake sediments, and tephra-fall deposits interlayered within the organic lake sediments (Fig. 3).

4.1. Pre-lake deposits (Hinuera Formation)

The oldest unit preserved in the core records comprised unconsolidated, brownish–greyish clays and clayey silts. This unit exhibited a massive soil texture with minor horizontal stratification and was only observed in six out of ten lakes within the Hamilton lowlands. In any event it was not involved in any soft-sediment deformation (Fig. 3c).

The unconsolidated clays and clayey silts of this unit were interpreted as pre-lake alluvial deposits of the Late Pleistocene Hinuera Formation (Schofield, 1965; Hume et al., 1975; Kear and Schofield, 1978). The Hinuera Formation refers to a thick (up to 90 m) heterogeneous unit of secondary volcaniclastic (Di Capua et al., 2022) gravelly sands, sandy gravels, sands, silts, and peat beds that form an alluvial plain within the Hamilton lowlands. Gravel-sized material was found to be dominated by fragments of rhyolitic breccia, rhyolite, pumice and ignimbrite, whereas sand and silt fractions were dominated by volcanic quartz, oligoclase/andesine plagioclase, pumice, and glass shards (Hume et al., 1975). The unconsolidated clays and clayey silts were likely deposited from suspension in abandoned braided channels and flood basins (Hume et al., 1975).

4.2. Organic lake sediment

The main sedimentary unit preserved in the core records comprised unconsolidated, massive, olive–grey, dark brown to black, organic clayey silt. It hosted the tephra layers that exhibited SSDSs. The organic content of this sediment ranged between 16 and 20 wt% and bulk densities were commonly exceptionally low, with wet densities of $\rho \approx 1100\,kg/m^3$ and dry densities of $\rho_d \approx 300\ kg/m^3$. The organic lake sediment was classified as highly compressible organic silt (OH) of low plasticity based on the Unified Soil Classification System (ASTM D2487-06, 2010), with an average plastic limit of $w_P = 119\%$ and liquid limit of $w_L = 301\%$.

The organic clayey silts were deposited in late Quaternary, typically dystrophic, lake environments and were found to be rich in humic material, being mainly classified as dy-gyttja and gyttja, or peat in shallow-water cores (Green and Lowe, 1985).

4.3. Tephra deposits

Eight prominent tephra layers were identified in the cores and correlated between lakes (Fig. 3c) using their stratigraphic positioning, physical properties, mafic and felsic mineralogical assemblages, and glass-shard major element compositions (Lowe, 1988b). Seven of these tephras (Taupō, Tuhua, Mamaku, Opepe, Waiohau, Rotorua, and Rerewhakaaitu) were rhyolitic, with colours ranging from white to light grey, and one (Mangamate tephra) was andesitic, and dark grey to dark olive in colour. They range in age from ~17.5 cal ka to ~1.7 cal ka BP (ages from Lowe et al., 2013). Each of the tephras is consistent in its mineralogical assemblages (dominated by volcanic glass, both vesicular and non-vesicular, with subordinate felsic and mafic minerals) across lakes in the lowlands (Lowe, 1988b). This lack of spatial variability in mineralogical assemblages is expected, given that these are distal tephras >100 km from their source vents (e.g., Juvigné and Porter, 1985; Lowe, 1988a; Alloway et al., 2013).

The observed tephra deposits commonly comprise horizontally bedded layers with distinctive boundaries with under- and overlying organic lake sediments (Fig. 3b). Taupō tephra, being the youngest tephra deposited at ~1.7 cal ka, was commonly only 1–3 mm thick and was therefore not considered further. The other seven tephra layers exhibited average thicknesses between 8 mm (i.e., Rerewhakaaitu tephra) and 44 mm (i.e., Rotorua tephra). Each of the tephra layers contained internal beds characterised by different grain sizes, varying between silt (i.e., extremely fine ash) and medium sand (i.e., medium ash). Except for Mangamate tephra, the tephra layers commonly had an upper silt bed, typically up to several millimetres thick. The upper silt bed was underlain by coarser beds, the number and grain size varying between tephras.

Tephra layers were grouped (groups I–III) according to their total thickness and internal bedding characteristics (Fig. 3b). Group I tephras included Opepe (Op), Waiohau (Wh), and Rerewhakaaitu (Rk). They were thin (between 8 and 13 mm thick) and commonly exhibited only two dominant beds, which we designated by numbers: an upper silt bed (e.g., Op-1, Wh-1, and Rk-1) underlain by a fine sand bed (e.g., Op-2, Wh-2, and Rk-2). In Waiohau tephra, two additional beds were observed in some lakes underlying the fine sand bed (Wh-3 and Wh-4). Group II tephras included Mangamate (Mm) (commonly 11 mm thick), which comprised up to five beds with the central medium sand bed (Mm-3) being the thickest one. Group III tephras included the remaining three tephras, Tuhua (Tu), Mamaku (Ma), and Rotorua (Rr), which were significantly thicker (21–44 mm) than the other tephra layers. The group III tephras commonly comprised five main internal beds as follows (from top to base): an upper silt bed (Tu-1, Ma-2, Rr-1), a very fine to fine sand bed (Tu-2, Ma-3, Rr-2), a medium sand bed (Tu-3, Ma-4, Rr-3), a thin silt bed (Tu-4, Ma-5, Rr-4), and a very fine to fine sand bed at the base (Tu-5, Ma-6, Rr-5).

The variability in thicknesses of tephra layers and their internal beds was studied for the cores taken from the ten lakes considered in our study (Fig. 4). For the majority of tephra layers (i.e., Mamaku, Opepe, Waiohau, and Rerewhakaaitu), the thicknesses of the tephra layers and their internal beds were similar throughout the Hamilton lowlands. Mangamate tephra, exhibiting similar thicknesses throughout the Hamilton lowlands, was typically dominated by the central medium sand bed (Mm-3), but the full sequence of internal beds was only present at one lake (Lake Rotokaeo, C2). The remaining tephras (Tuhua and Rotorua) exhibited larger variability in tephra thickness.

The overall thickness of Tuhua tephra varied between 20 mm (in Lake Rotoroa, C1) and 42 mm (in Leeson's Pond, N3). A slight directional trend could be observed in the overall thickness of Tuhua tephra (Fig. 5). The thickness of Tuhua tephra seemed to increase from south to north. This observation is in accordance with maps in

Lowe (1988b) and Hopkins et al. (2021). The internal bedding characteristics of Tuhua tephra differed with overall tephra thickness. We observed that thicker layers commonly exhibited the full set of internal beds (Tu-1 to Tu-5), whereas the thinner layers lacked some of the internal beds. For example, in Lake Rotokaraka (N2) only internal beds Tu-2 to Tu-4 could be observed.

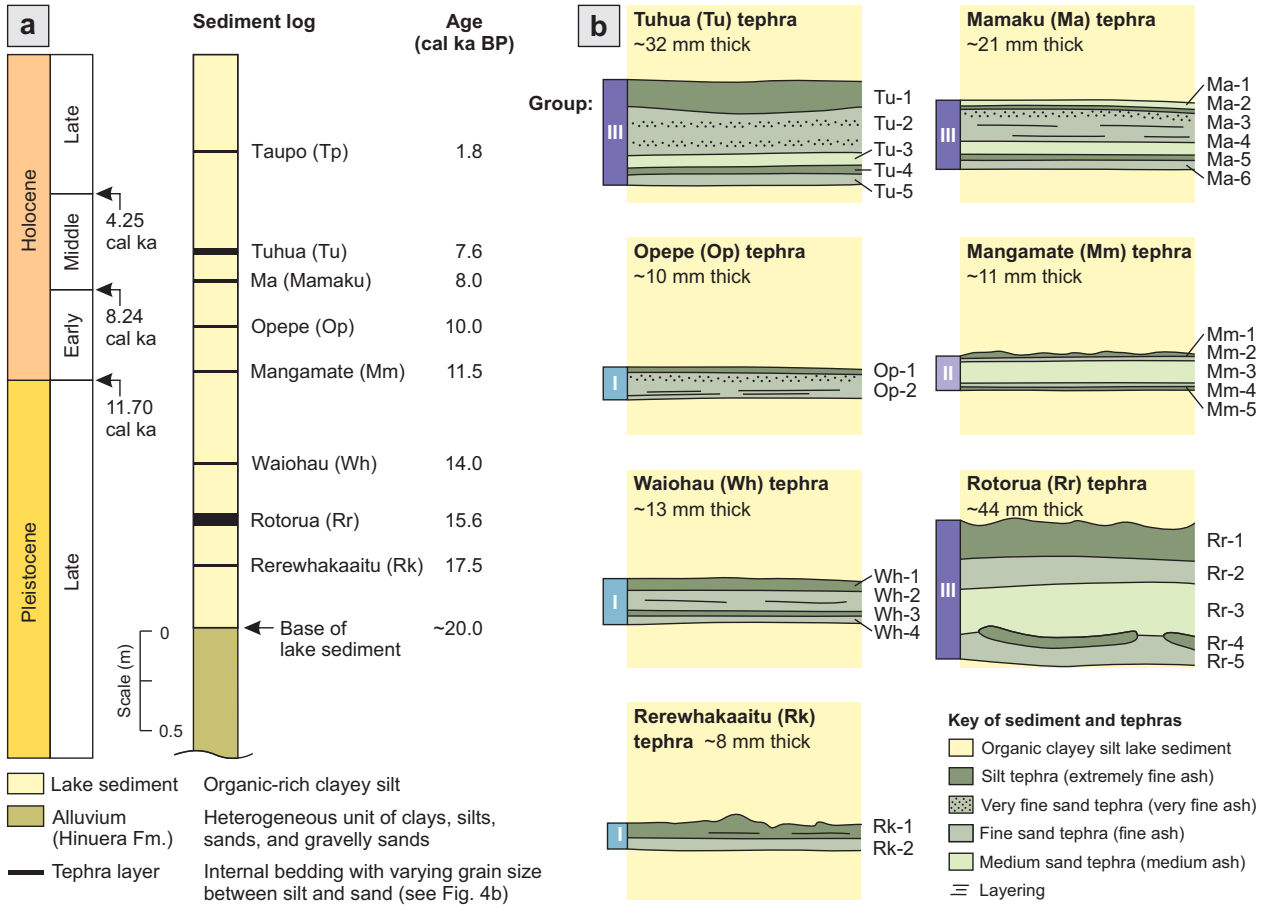

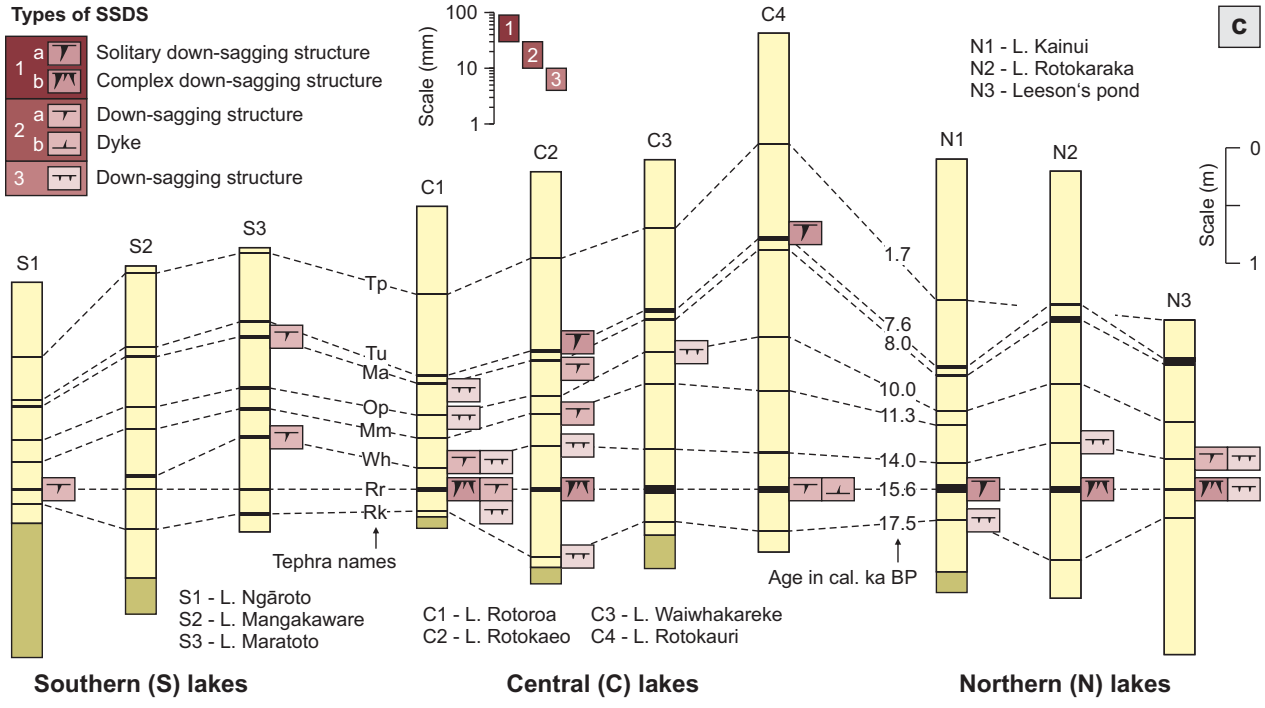

The overall thickness of Rotorua tephra varied between 25 mm (in Lake Rotoroa, C1) and 77 mm (in Lake Kainui, N1). A slight directional trend could also be observed for Rotorua tephra, increasing in thickness towards the north-west. This observation is contradictory to trends in the published literature (Nairn, 1980; Lowe, 1988b). For Rotorua tephra, the thickness of internal beds was linked to the overall thickness of the tephra layer (with the exception of Lake Waiwhakareke, C3). For example, the thickness of the upper silt bed increased with overall thickness, but the proportions between internal beds remained more or less constant.

5. Description of SSDSs

All seven major tephra layers exhibited SSDSs in the form of mainly elongated load structures (i.e., down-sagging structures), dykes, and collapse structures, their occurrence and dimensions being variable throughout the Hamilton lowlands (Fig. 3c). SSDSs were differentiated into three main types based on their dimensions, ranging between 30–100 mm (type 1), 10–30 mm (type 2), and <10 mm (type 3).

5.1. Type 1a solitary down-sagging structures

The term 'type 1a solitary down-sagging structure' was used to describe elongated, ~30–100-mm long, solitary load structures that intruded (from the tephra layer) into underlying organic lake sediments. This type of SSDSs was observed in six tephra layers and was restricted to deformations in the relatively thick Tuhua and Rotorua tephras deposited in central and north-western lakes (i.e., Rotokaeo, C2; Rotokauri, C4; Kainui, N1) (Figs. 1a, 3c).

Fig. 6 shows two typical examples of type 1a solitary down-sagging structures by means of core photos, our interpretation of internal beds and deformation features, and CT images from the outside of the whole-round core and as a longitudinal slice through the centre of the core. In the CT images, the organic lake sediment was removed using a high-pass filter. The organic lake sediment and SSDSs sometimes exhibited similar CT densities. Therefore, it was not always possible to remove the entire organic lake sediment from CT datasets. As a result, the SSDSs shown in CT images are slightly larger than those shown in the core photos. The two typical examples of type 1a solitary down-sagging structures (Fig. 6) are also available as rotational 360-degree videos in Supplementary Videos S1–S4.

The deformation involved all internal tephra beds (except for the upper silt beds Rr-1 and Tu-1) and underlying organic lake sediment. Type 1a solitary down-sagging structures shown in Fig. 6 were commonly up to 10-mm wide and up to 80-mm long, deformation features, which decreased in width towards the base. They exhibited sharp, distinct boundaries with surrounding organic lake sediment. Down-sagging structures appeared to be sheet-like in CT images and resembled load casts (sensu Owen, 2003). Disruptions of the thin silt beds (Rr-4, Tu-4) and underlying very fine to fine sand beds (Rr-5, Tu-5) indicate that the infill material of the down-sagging structure originated from the upper very fine to fine sand beds (Rr-2, Tu-2) or medium sand bed (Rr-3), or both.

The down-sagging structure Rr-6, which formed in the Rotorua tephra layer (Fig. 6a), exhibited a sheet-like geometry with vertical orientation and pointed end, whereas in the Tuhua tephra layer (Fig. 6b), three sheet-like down-sagging structures (Tu-6, Tu-7, Tu-8) were present, one of them (Tu-8) inclined at ~45°, and all extending down towards Mamaku tephra, the latter occurring ~80 mm below the Tuhua tephra layer. In addition to the three down-sagging structures, a small normal fault with an offset of ~4 mm was observed in the lower beds of Tuhua tephra (Tu-4, Tu-5).

A collapse structure (C-1) was observed in the Tuhua tephra shown in Fig. 6b. Here, organic lake sediment overlying the tephra layer collapsed into the upper silt bed (Tu-1), corresponding to the down-sagging structure Tu-6 below.

5.2. Type 1b complex down-sagging structures

The term 'type 1b complex down-sagging structure' was used to describe heterogeneous, ~30–100-mm long, often interconnected load structures that intruded from tephra layers into underlying organic lake sediments. This type of SSDSs was observed in ten tephra layers and was restricted to deformations in Rotorua tephras deposited in central and north-eastern lakes (i.e., Rotoroa, C1; Rotokaeo, C2; Rotokaraka, N2; Leeson's Pond, N3) (Figs. 1a, 3c).

Fig. 7 shows three typical examples of type 1b complex down-sagging structures. One of those examples is also available as rotational 360-degree videos in Supplementary Videos S5–S6. Similar to the type 1a SSDSs, the type 1b complex down-sagging structures involved deformations in all internal beds of Rotorua tephra (except for the upper silt bed Rr-1) and the underlying organic lake sediment. Furthermore, down-sagging structures exhibited sharp, distinct boundaries with surrounding organic lake sediment. The infill material of the down-sagging structures originated from the upper very fine to fine sand beds (Rr-2) or medium sand bed (Rr-3), or both.

Individual type 1b complex down-sagging structures shown in Fig. 7 were commonly 2–3 mm wide and up to 90 mm long (with most down-sagging structures being ~30–40 mm long) with pointed ends. Down-sagging structures were found to resemble load casts and pseudonodules (sensu Owen, 2003) in the split core. However, when considering the volumes of tephra and SSDSs in CT scans, in which the less-dense organic lake sediment had been removed, down-sagging structures appeared to be continuous and no pseudonodules could be observed. Individual deformations, together forming the type 1b complex down-sagging structures, were observed to be curved (e.g., Rr-7), wavy (e.g., Rr-10), or straight (e.g., Rr-8, Rr-15, Rr-17), and often oriented vertically or at an angle between 90° (vertical) and 0° (horizontal). In one example (Rr-13), flame-like structures were observed within the down-sagging structure, being directed upwards, horizontally, as well as downwards. Sometimes (e.g., Rr-16), the down-sagging structure consisted of a main deformation feature from which and a number of smaller sub-deformations originate.

Distinct collapse structures (C-2 to C-5) were observed at the boundary between organic lake sediment and the tephra layers. Collapse structures corresponded to deformations within internal tephra beds below. For example, the collapse structure C-2 corresponded to the type 1b complex down-sagging structures Rr-8 and Rr-9 (Fig. 7a). As a consequence of multiple collapse structures, the upper interface between the tephra layer and organic lake sediment appeared flame-like rather than straight (e.g., Fig. 7a). In one case (C-4, Rr-13), the organic lake sediment collapsed down into very fine to fine sand and medium sand beds (Rr-2, Rr-3), resulting in a normal fault with an offset of ~40 mm within the upper silt bed (Rr-1).

Fig. 3. (a) Stratigraphy of eight prominent tephra layers deposited in lakes throughout the Hamilton lowlands. The Pleistocene-Holocene boundary and the subdivisions of the Holocene follow Walker et al. (2009) and Walker et al. (2019), respectively. (b) Sedimentary facies of the seven most relevant tephra layers showing nomenclature, grain size classes, and thicknesses of internal beds used throughout the present study. Tephra layers were grouped (groups I–III) based on their thickness and internal bedding characteristics. (c) Correlation of post-20-cal-ka major tephra layers between northern, central, and southern lakes within the Hamilton lowlands, indicating the different types of SSDSs observed in specific tephra layers. Tephra names (Froggatt and Lowe, 1990; Moebis et al., 2011) and volcanic sources (in parentheses: see Fig. 1c) are as follows: Tp = Taupō (TVC); Tu = Tuhua (TuVC); Ma = Mamaku (OVC); Op = Opepe (TVC); Mm = Mangamate (TgVC); Wh = Waiohau (OVC); Rr = Rotorua (OVC); Rk = Rerewhakaaitu (OVC). Ages of tephras are from Moebis et al. (2011), Lowe et al. (2013), and Lowe et al. (2018).

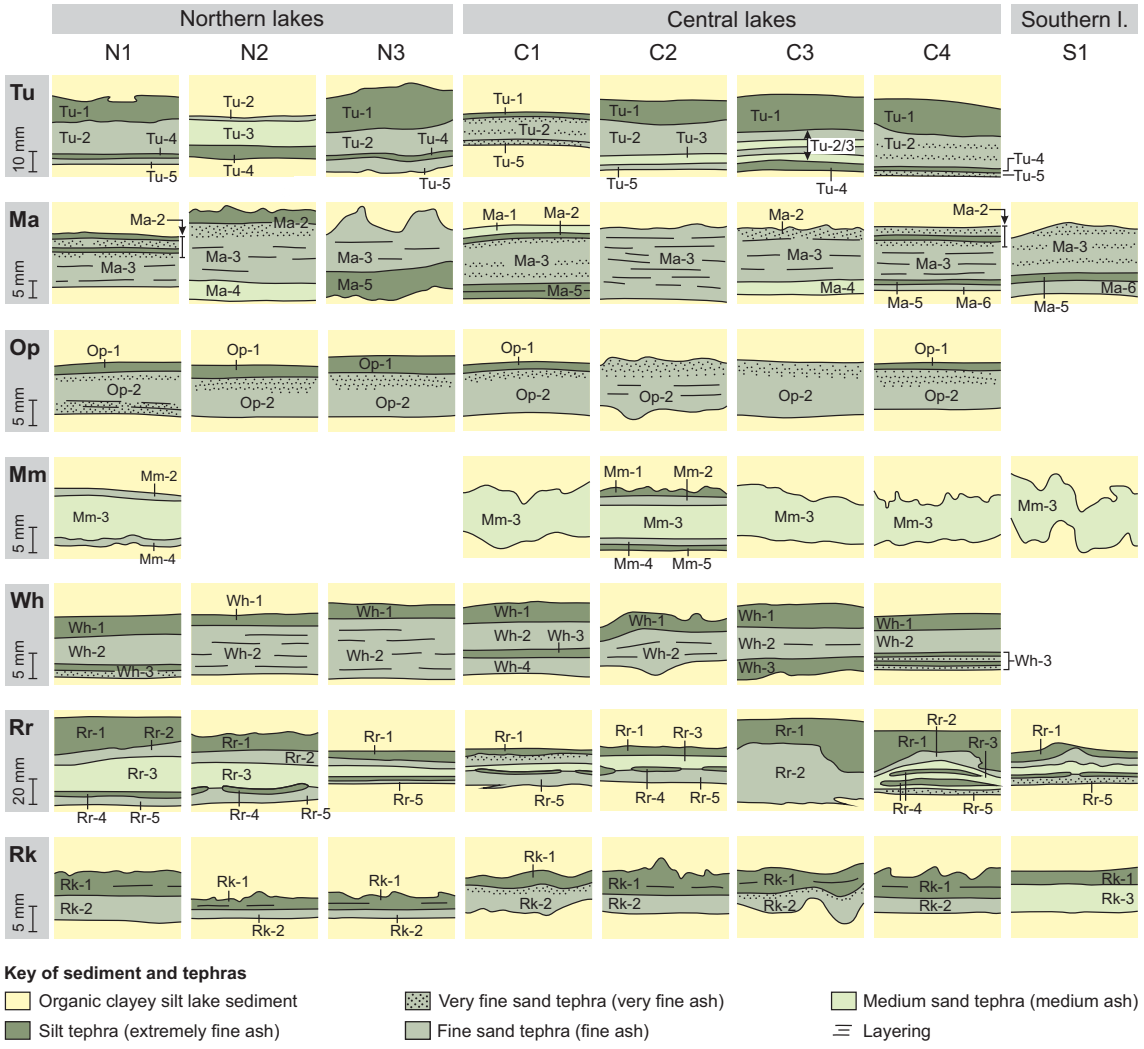

Fig. 4. Variability of tephra thickness and internal bedding characteristics between lakes. Note that internal bedding characteristics were not available for every tephra layer and lake due to lack of a specific tephra in that lake or due to incomplete sediment description. Full lake and tephra names are provided in Figs. 1a and 3a.

5.3. Type 2a down-sagging structures

The term 'type 2a down-sagging structure' was used to describe ~10–30-mm long load structures that intruded from a tephra layer downwards into underlying organic lake sediments. Thirteen of this type of SSDSs were observed across various lakes (Ngāroto, S1; Maratoto, S3; Rotoroa, C1; Rotokaeo, C2; Rotokauri, C4; Leeson's Pond, N3; Fig. 1a). They occurred in Mamaku, Mangamate, Waiohau, and Rotorua tephras (Fig. 3c).

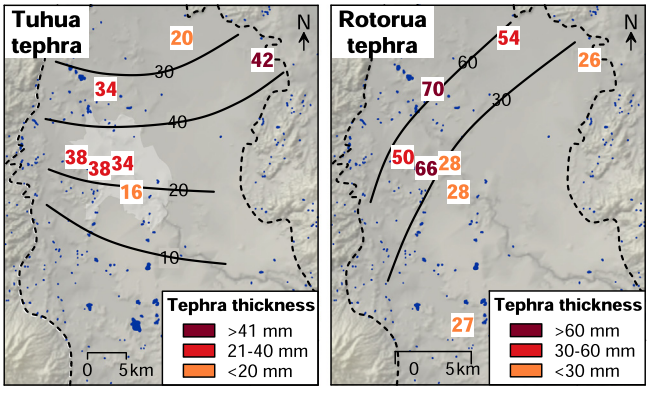

Fig. 5. Variability in thickness of Tuhua (Tu) and Rotorua (Rr) tephras within the Hamilton lowlands. The orientation of thickness contours (black solid lines) follow Lowe (1988b).

Fig. 8a–b shows typical examples of type 2a down-sagging structures. The down-sagging structure (Wh-4) involved deformations within the very fine to fine sand bed (Wh-2), underlying silt bed (Wh-3), and organic lake sediment below the tephra layer (Fig. 8a). The down-sagging structure was ~15 mm wide and ~15 mm long and decreased in width towards the bottom. The boundary between the down-sagging structure and the organic lake sediment was slightly more diffuse compared with that for the type 1 down-sagging structures. A distinct collapse structure (C-6) was also associated with this type 2a down-sagging structure. Further type 2a down-sagging structures were observed in Rotorua tephra (Fig. 8b). Here, tephra material from the medium sand bed (Rr-3) intruded downwards through basal tephra beds (Rr-4, Rr-5) forming two down-sagging structures (Rr-19, Rr-20). Rr-19 was ~15 mm wide and ~20 mm long and exhibited a rounded end, whereas Rr-20 was narrow and appeared discontinuous in the split core photo. Both down-sagging structures comprised load casts and pseudonodules, the latter likely being a result of the location of the plane of observation relative to the SSDSs.

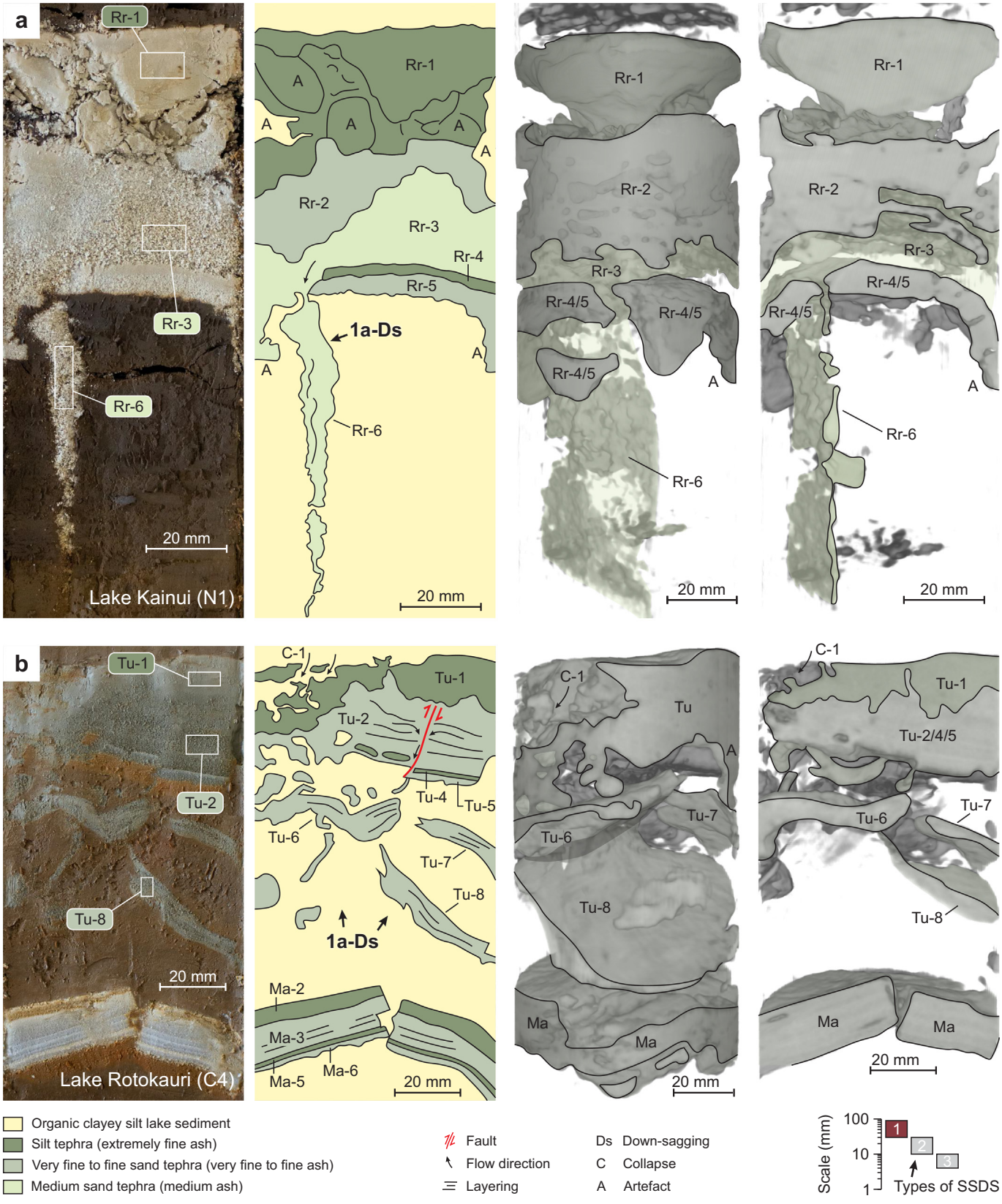

Fig. 6. SSDSs in the shape of 30–100-mm long, type 1a solitary down-sagging structures observed in (a) Rotorua (Rr) and (b) Tuhua (Tu) tephras. Panels show (from left to right) core photos, interpretations of internal bedding and deformation structures, and CT images of the tephra layer and its deformation structures (with the organic lake sediment removed using a high-pass filter) from the outside of the whole-round core and as a longitudinal slice through the centre of the core. (a) Down-sagging structure (Rr-6) intrudes from medium sand bed (Rr-3) through basal beds (Rr-4, Rr-5) into underlying organic lake sediment. Note that the fractured appearance of the upper silt bed (Rr-1) is considered to be a coring artefact (i.e., A) and does not represent deformation during the SSDS formation. (b) Three down-sagging structures (Tu-6, Tu-7, Tu-8) intrude from very fine to fine sand bed (Tu-2) through basal beds (Tu-4, Tu-5) into underlying organic lake sediment. Ma = Mamaku tephra. Labels and boxes in left panel indicate locations chosen for grain size sampling.

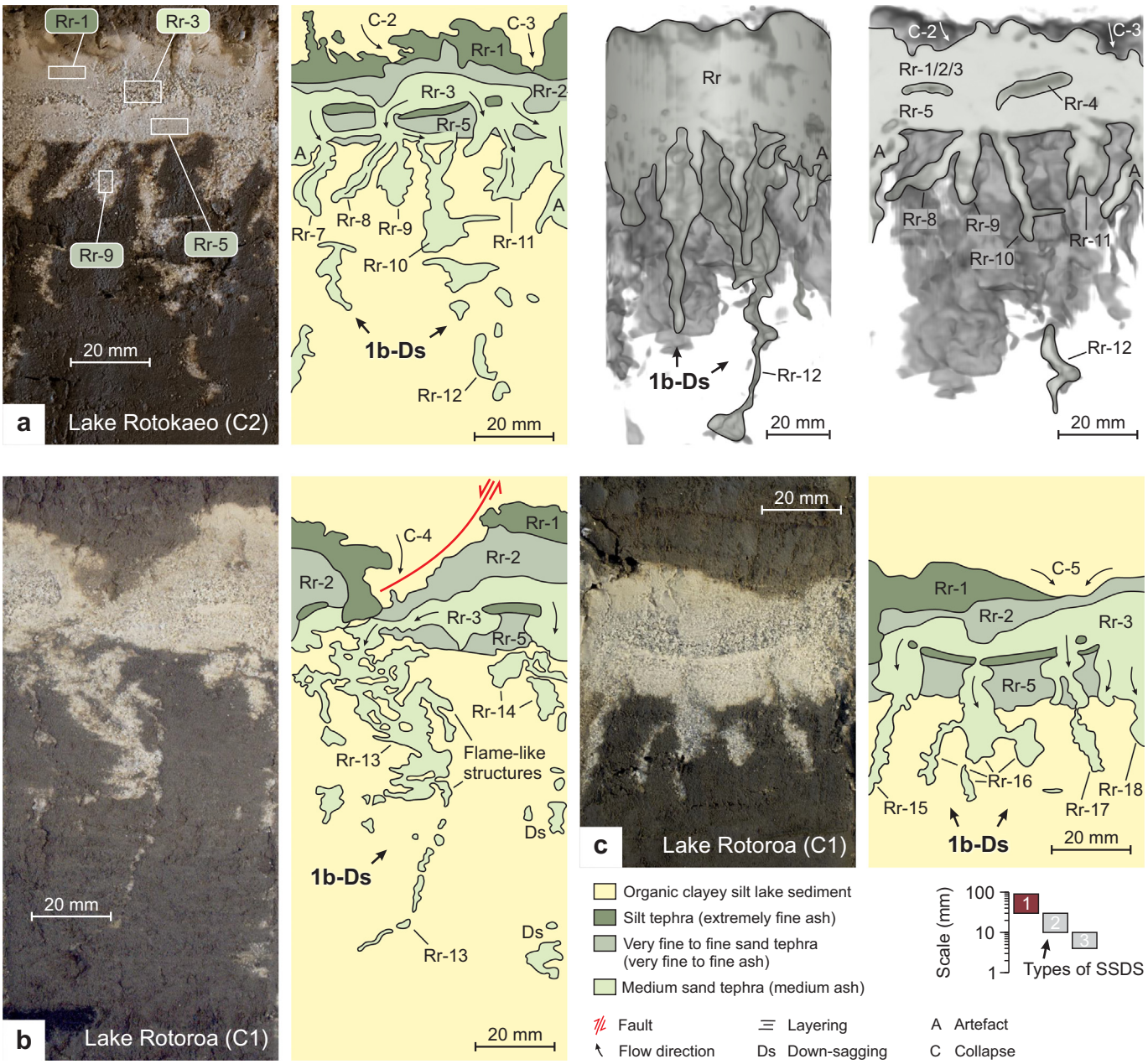

Fig. 7. SSDSs in the shape of 30–100-mm long, type 1b complex down-sagging structures in Rotorua (Rr) tephra. Panels show (from left to right) core photos, interpretations of internal bedding and deformation structures, and (in (a) only) CT images of the tephra layer and its deformation structures (with the organic lake sediment removed using a high-pass filter) from the outside of the whole-round core and as a longitudinal slice through the centre of the core. Down-sagging structures (Rr-7 to Rr-18) intruding from medium coarse sand bed (Rr-3) through basal beds (Rr-4, Rr-5) into underlying organic lake sediment. Numerous collapse structures (C-2 to C-5) corresponded with deformations within tephra beds and indicate loss in tephra volume due to the process of down-sagging of tephra material. The labels and boxes in the upper left panel indicate locations chosen for grain size samples.

5.4. Type 2b dyke

The term 'type 2b dyke' was used to describe ~10–30-mm long upward-directed intrusions from a tephra layer into the upper silt bed within the tephra layer. Two of this type of SSDSs were observed at two lakes (Rotoroa, C1; Rotokauri, C4; Fig. 1a). They occurred in Waiohau and Rotorua tephras (Fig. 3c).

A type 2b dyke (Wh-5) was observed within the Waiohau tephra, which also provided the source of the type 2a down-sagging structure Wh-4 (Fig. 8a). The dyke, which originated from the very fine to fine sand bed (Wh-2), was ~10 mm wide, ~15 mm long, and inclined at ~45°. It seemed that the upper silt bed (Wh-1) was lifted upwards as a consequence of the deformation process of dyke Wh-5. A second type 2b dyke (Rr-21) was observed in Rotorua tephra (Fig. 8c). Here, tephra from the very fine to fine sand bed (Rr-2) intruded upwards into the upper silt bed (Rr-1), where it stopped propagating in the middle of the silt bed. The dyke was 18 mm wide, 25 mm long, slightly curved, and tapered upwards.

5.5. Type 3 down-sagging structures

The term 'type 3 down-sagging structure' was used to describe small, <10-mm long, load structures that intruded from the tephra layer downwards into underlying organic lake sediments. Type 3 down-sagging structures were observed in nine tephra layers and occurred in Mamaku, Opepe, Waiohau, Rotorua, and Rerewhakaaitu

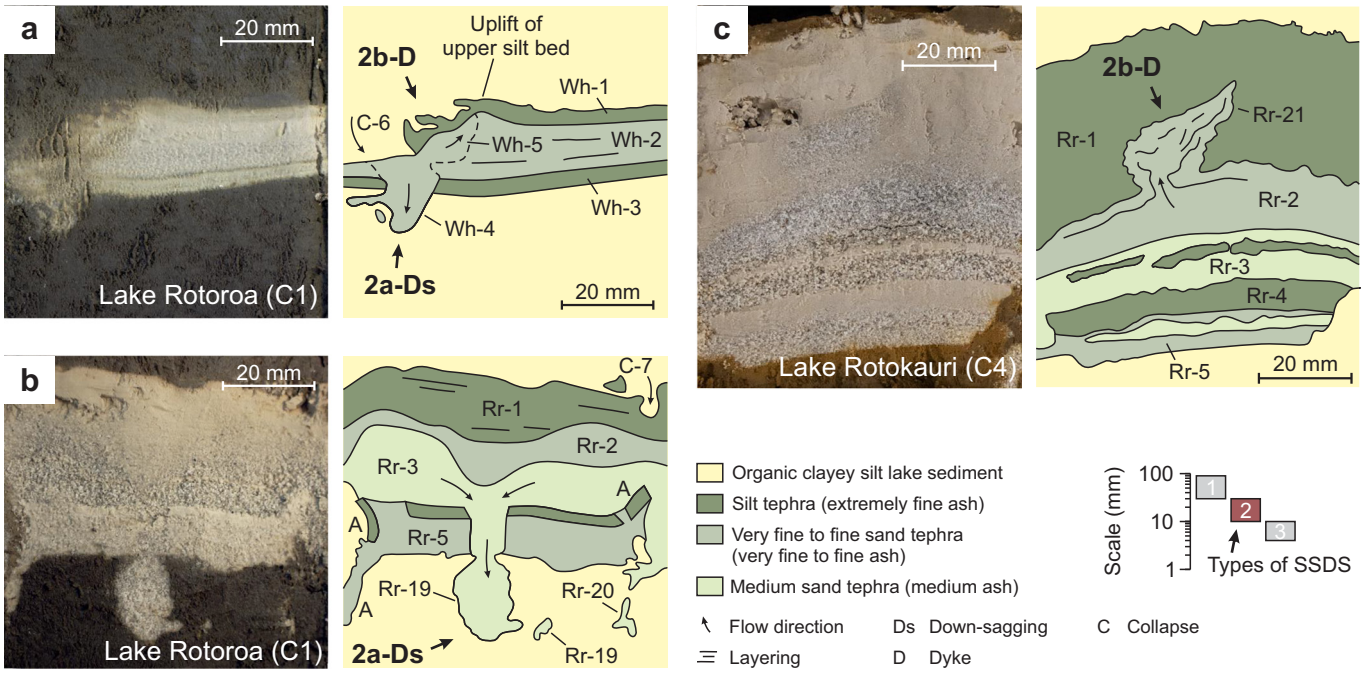

Fig. 8. SSDSs in the shape of 10–30-mm long, type 2a down-sagging structures (a–b), and type 2b dykes (a, c) observed in (a) Waiohau (Wh) and (b–c) Rotorua (Rr) tephras. Panels show (from left to right) core photos and interpretations of internal bedding and deformation features. (a) Type 2a down-sagging structure (Wh-4), with associated collapse structure (C-6), intruding from very fine to fine sand bed (Wh-2) through the basal silt bed (Wh-3) into underlying organic lake sediment. A type 2b dyke (Wh-5) was observed in the same tephra layer, intruding upwards within very fine to fine sand bed (Wh-2). (b) Tephra intruded from medium sand bed (Rr-3) through basal beds (Rr-4, Rr-5) forming two type 2a down-sagging structures (R-19, R-20). (c) Type 2b dyke (Rr-21) intruding from very fine to fine sand bed (Rr-2) into silt bed above (Rr-1).

tephras deposited in central and northern lakes (i.e., Rotoroa, C1; Rotokaeo, C2; Waiwhakareke, C3; Kainui, N1; Rotokaraka, N2; Leeson's Pond, N3) (Figs. 1a, 3c).

Type 3 down-sagging structures were found to be irregularly shaped, downward-directed intrusions into underlying organic lake sediment, forming load casts (e.g., Ma-7, Wh-10) or pseudonodules (e.g., Ma-8, Wh-11). Pseudonodules appeared as small lumps (commonly up to ~5 mm long) entirely separated from the tephra layer. Down-sagging structures were commonly associated with the collapse of overlying organic lake sediment into the tephra layer (e.g., C-8, Ma-7; C-15, Wh-11).

6. Interpretation of SSDSs

The different types of SSDSs found in tephra deposits in the lakes within the Hamilton lowlands were interpreted by firstly establishing a deformation mechanism and driving force system and then providing evidence for the most likely triggering mechanism using both the context-based and criteria-based approaches (Owen and Moretti, 2011; Owen et al., 2011).

6.1. Deformation mechanism

The SSDSs analysed in the present study (i.e., down-sagging structures and dykes) are commonly interpreted to be a consequence of liquefaction, although a number of other processes may also produce similar deformations in the sedimentary record (Moretti and van Loon, 2014). Liquefaction is a failure process that commonly occurs in water-saturated, loosely compacted granular materials. In those materials, shear stresses (e.g., from earthquake-induced shaking or rapid burial) may cause the grain fabric to collapse and become compact, leading to strength loss and temporary transfer of stress from the grain-to-grain contacts to the pore water. In environments where pore water pressure is prevented from dissipating, shear stresses may lead to a complete transfer of stress to the pore water, resulting in strength loss and viscous fluid-like behaviour of the granular material, with little or no yield strength (Owen and Moretti, 2011).

A number of compositional and geological characteristics define whether or not a sediment may be considered susceptible to liquefaction (Kramer, 1996). Compositional characteristics include the grain size distribution and the packing density (i.e., relative density) of the sediment (or tephra deposit). Liquefaction is commonly restricted to coarse silt to fine sand deposits (Moretti et al., 1999), although exceptions exist where liquefaction has been observed in gravelly soil (Cubrinovski et al., 2017; Zhou et al., 2020). Fine to medium silt is commonly considered less-liquefiable than coarse silt and sand (although cases exist, such as that of Ishihara, 1985), especially when clay minerals are present, preventing the collapse of the grain fabric during shearing (Boulanger and Idriss, 2006). In our study, SSDSs were only observed in very fine to fine sand and medium sand tephra beds, whereas the upper silt beds and encapsulating organic lake sediments were not directly involved in the deformation process: the upper silt bed was passively involved in the collapse of organic lake sediment overlying the tephra layer and the organic lake sediment below the tephra layer deformed because of the intrusion of SSDSs. Grain size distribution curves were obtained for the organic lake sediment, and for the upper silt beds (where applicable) and deformable beds (i.e., tephra source beds from which SSDSs were initiated) of each of the seven major tephra layers (Fig. 10). For some thick tephra layers comprising SSDSs (i.e., Tuhua, Rotorua), grain size distribution curves could also be obtained for the type 1a down-sagging structures. We observed from these plots that the grain size distributions of the organic lake sediment and upper silt beds exhibited a large proportion of fines and were therefore systematically located outside the range for liquefiable soils defined by Tsuchida (1970), these ranges being widely used to distinguish liquefiable from less-liquefiable soils (Moretti et al., 1999; Rodríguez-Pascua et al., 2016; Villamor et al., 2016). The grain size distribution curves of deformable beds and down-sagging structures were mostly located within the liquefiable or potentially liquefiable ranges (Fig. 10).

The packing of the sediment (including tephra in our case) is another compositional characteristic governing liquefaction susceptibility (Owen and Moretti, 2011). Liquefaction develops most readily in loosely packed deposits, because when sheared, these become compacted and produce a more pronounced pore water pressure than more densely packed deposits. The packing (i.e., relative density) of individual internal tephra beds could not be directly assessed in the present study because of the relatively large amount of tephra material needed to perform the required laboratory tests from which relative density would be derived (i.e., dry bulk density, minimum and maximum dry density tests, DIN 18126, 1996). The finely bedded tephra-fall layers were deposited through water soon after being explosively erupted and carried by wind from source volcanoes (Fig. 1c). It is very likely that the internal bedding in the tephra layers largely reflects primary atmospheric dispersal and fallout processes (e.g., Alloway et al., 2013; Hopkins et al., 2015; Mastin et al., 2023) rather than substantial re-sorting or potential reworking during, or after, falling through the shallow lake-water columns: in the Hamilton lowlands, the lakes are closed-basin and ground-penetrating radar evaluation (Lowe, 1985) has shown (in Lake Maratoto) that individual, discrete tephra layers follow lake basin contours, a characteristic of tephra-fall beds (Houghton and Carey, 2015). Water sedimentation of quartz sand has been found to form deposits of medium densities (Wood et al., 2008). It is unknown how tephra-derived particles, overwhelmingly dominated by volcanic glass shards (Lowe, 1988b, 1988a) and having a low particle density, large surface roughness, and usually high vesicularity, would deposit through water, but it may be expected that pumiceous tephra particles will form looser grain fabrics, within the loose to medium density range, than quartz sand.

Geological characteristics used for liquefaction susceptibility assessments include the sedimentary environment, groundwater conditions, age of deposition, and depth of burial (Youd, 1991). Fluvial, estuarine, and aeolian sediments are more often found to have liquefied because such materials occur in sedimentary environments that favour deposition of loose and well-sorted fine to medium sands (Kramer, 1996). The sedimentary environment may also control the presence of permeability barriers within the sedimentary succession, such as mud layers, which increase the chance of liquefaction by creating zones of elevated pore water pressures (Obermeier, 1996; Owen and Moretti, 2011). The sedimentary environment in our study (i.e., lacustrine, together with tephra-fall deposition) favoured water-saturated successions of relatively loosely packed, relatively thin tephra deposits interlayered with fine-grained organic lake sediments. Furthermore, the sedimentation (atmospheric fallout) process of tephra layers generated the internal tephra bedding, typically with an upper silt bed at the top. It is plausible that the organic lake sediment above and below the tephra as well as the upper silt bed acted as permeability barriers and therefore increased the susceptibility to liquefaction in the very fine to fine and medium sand tephra beds. Deformation in Mangamate tephra was observed in only one lake (Lake Rotokaeo, C2). In this lake, Mangamate tephra exhibited an upper and lower silt bed. In all other lakes, Mangamate tephra was found to be intact and only consisted of the fine sand and medium sand beds (Mm-2 to Mm-4). Hence, it is concluded here that the lack of the upper silt bed in most lakes led to a lower liquefaction susceptibility for the Mangamate tephra layer.

Liquefaction susceptibility commonly decreases with time after deposition due to post-depositional processes, including cementation, consolidation, and compaction–the last two being the consequence of increase in overburden sediments with time. It has been shown that the liquefaction resistance of sandy soils increases by 40 % within 400 years after deposition because of cementation and grain dislocation (Towhata et al., 2017) and that most liquefaction is observed in sediments buried <5 m (Obermeier, 1996). The tephra layers in our lacustrine study were deposited since ~17.6 cal ka BP and their interlayering within permanently saturated (anoxic) organic lake sediments has prevented significant alteration by hydrolysis or other chemical weathering processes (e.g., Churchman and Lowe, 2012). The high analytical totals of major elemental analyses of glass shards from the lacustrine tephras (Lowe, 1988b), which are extremely vulnerable to rapid hydration and dissolution (e.g., Kirkman and McHardy, 1980; Wolff-Boenisch et al., 2004; Churchman and Lowe, 2012), show that the glasses remain essentially pristine (shown also in other lacustrine-tephra studies, e.g., Newnham et al., 2004; Hopkins et al., 2015; Watson et al., 2016). In addition, the presence of easily weatherable silicate minerals, including olivine, in the ferromagnesian mineral assemblages (Lowe, 1988b) also indicates a lack of weathering. Only in special circumstances, such as very high acidity, are glasses and mafic minerals susceptible to dissolution in anoxic environments (e.g., Hodder et al., 1991; Hodder et al., 1996). Hence, the tephra layers in our study have not undergone cementation, precluding a decrease in liquefaction susceptibility due to cementation.

Consolidation and compaction are similarly limited for the tephra layers in our study: they may be considered unconsolidated because the overburden stress is estimated to be very low (i.e., $\sigma_z < 20$ kPa) due to the low bulk densities of organic lake sediments; and deformations described in our study occurred in tephra layers buried by <4.5 m of organic lake sediments. Thus, the liquefaction susceptibility of these tephras is likely to have persisted since their deposition.

Since liquefaction involves the temporary transition of the sediment body from solid-like to viscous fluid-like behaviour, the ensuing deformation will be ductile in character. Brittle features may only be observed in sediment that was adjacent to liquefied material when the deformation took place (Owen and Moretti, 2011). The SSDSs observed in our study commonly featured ductile deformations characterised by internal flow structures (e.g., Figs. 6a, 7). Furthermore, SSDSs commonly penetrated through basal (internal) tephra beds into underlying organic lake sediments, indicating high pore water pressure within the source tephra beds in which deformation was initiated. The boundaries between SSDSs and organic lake sediments were found to be mostly brittle (although exceptions exist, e.g., the flame-like structure in type 1b down-sagging structure R-13), probably due to the low plasticity of the organic lake sediment. The upper silt beds exhibited collapse structures often associated with down-sagging structures below (e.g., Fig. 7). These collapse structures exhibited mainly ductile but also sometimes brittle deformations, indicating that the upper silt beds were at the transition between ductile and brittle soil behaviour.

The preceding discussion summarised the liquefaction-related compositional, geological, and morphological characteristics of organic lake sediments and tephra layers. It may be inferred here that the source tephra beds from which the deformation was initiated (i.e., very fine to fine sand and medium sand beds, equivalent to very fine to fine and medium ash beds in the volcanological grain size scale) exhibited considerably higher susceptibility to liquefaction than the upper silt beds (extremely fine ash beds) and organic lake sediments. We note that in order to obtain a holistic liquefaction susceptibility of the silt beds, Atterberg limits would have been required (Boulanger and Idriss, 2006). However, determining Atterberg limits on the internal tephra beds was not possible in our study due to the small volume of tephra material available. Liquefaction is evidently a feasible deformation mechanism for the SSDSs described in our study. In subsequent sections we assume that SSDSs reported here were caused by liquefaction.

6.2. Driving forces of deformation

6.2.1. Influence of tephra thickness on occurrence and type of SSDSs

The analyses of sedimentary facies and SSDSs revealed that the thickness of tephra layers and their internal beds varied somewhat throughout the lakes of the Hamilton lowlands (Fig. 4) and that deformation was commonly initiated within the very fine to fine sand and medium sand beds (e.g., Rr-2, Rr-3), but constrained by the upper silt bed (e.g., Rr-1), where deformation was limited to the collapse of organic lake sediments and upper silt beds into underlying tephra beds (Figs. 6–9). It may be

assumed that variations in thickness (i.e., available volume during the deformation process) of tephra layers and their internal beds may have therefore controlled the occurrence and type of SSDSs.

An initial assessment of the driving forces of deformation was performed by analysing the thicknesses of tephra layers and their internal beds and comparing them to the type and dimensions of SSDSs. The total tephra thickness h_{Tot} and the thicknesses of the upper silt bed h_{Silt} and liquefiable ('deformable' in previous sections) beds h_{Liq} were correlated to the dimensions of SSDSs by means of the average area (visible in the split core) and the maximal vertical length of individual SSDSs, respectively (Fig. 11). A fairly strong positive relationship was obtained for the correlation between the total tephra thickness and the average area of SSDSs, with a Pearson's correlation coefficient of $R = 0.91$ (Fig. 11a). Hence, we conclude that the average area of SSDSs linearly increases with the total tephra thickness. Furthermore, it was found that SSDSs occurred in tephra layers of at least ~8 mm thickness and that the type of SSDSs depended on the total tephra thickness and, thus, the available volume of liquefiable tephra material. Type 2 and 3 SSDSs, having the smallest dimensions of SSDSs analysed in our study, commonly occurred in tephra layers with total thicknesses less than ~20 mm (with some exceptions). Type 1b complex down-sagging structures exhibited larger dimensions and occurred in tephra layers of intermediate thickness (~30 mm). Type 1a solitary down-sagging structures exhibited the largest dimensions and occurred in tephra layers at least ~40 mm in thickness.

The thickness of the upper silt bed and the thickness of the liquefiable bed(s) correlated with the average area of SSDSs too, with Pearson's correlation coefficients of $R = 0.91$ and $R = 0.70$, respectively (Fig. 11b–c). The fairly strong correlation between the thickness of the upper silt bed, which was not directly involved in the liquefaction process, and the average area of SSDSs, is considered here to be a result of the intrinsic relationship between the total tephra thickness and the thickness of its internal beds. It may be expected that with an increase in total tephra thickness, the thicknesses of internal beds would increase likewise, keeping the proportions more or less constant. This latter relationship can be directly observed, especially in Rotorua tephra (Fig. 4). The maximal vertical length of SSDSs was only moderately correlated with the thickness of liquefiable bed(s) (Fig. 11d). Therefore, the maximal vertical length of SSDSs is considered less suitable for assessing the dimensions and type of SSDSs for a given tephra layer.

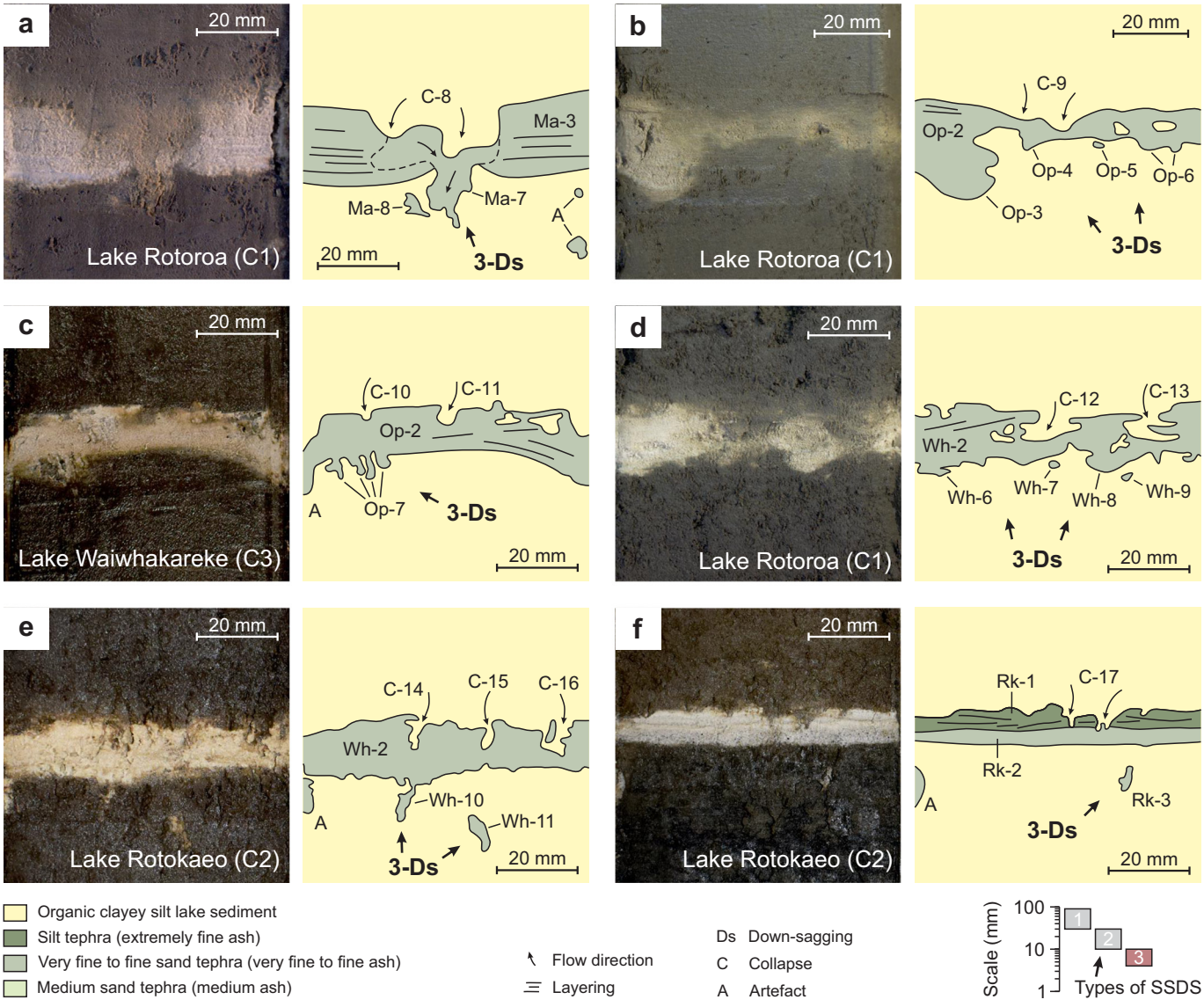

Fig. 9. SSDSs in the shape of <10-mm long, type 3 down-sagging structures present in various tephras and lakes with collapse structures (C-8 to C-17) indicating loss of tephra volume due to the processes of deformation. Tephra abbreviations: Ma = Mamaku; Op = Opepe; Wh = Waiohau; Rk = Rerewhakaaitu.

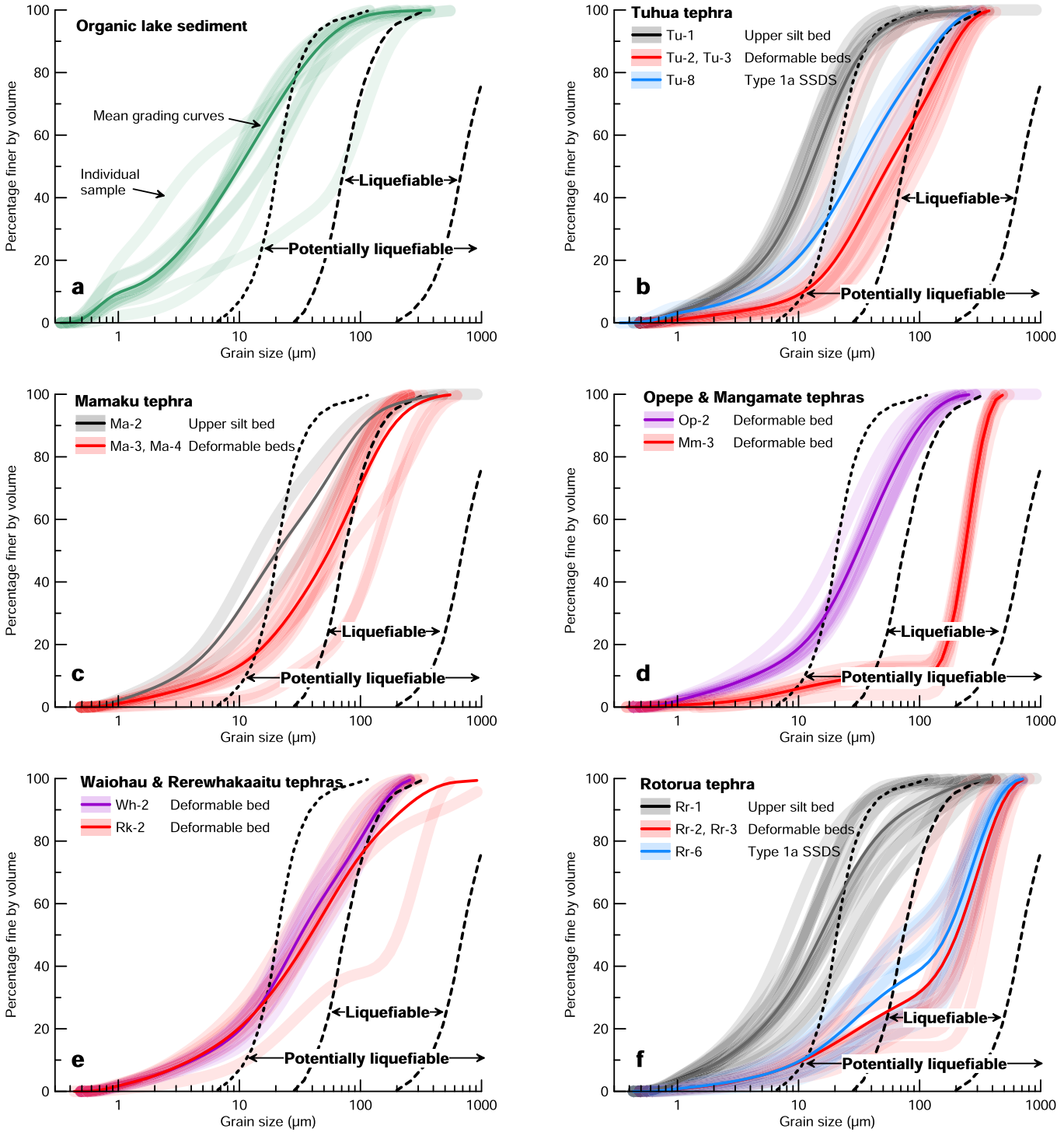

Fig. 10. Grain size distribution curves of (a) organic lake sediment and (b–f) tephra layers. If applicable, grain size distribution curves were distinguished for upper silt beds, deformable beds, and SSDSs. Boundaries for liquefiable and potentially liquefiable soils are from Tsuchida (1970). In each plot, transparent and solid curves indicate individual and averaged grading curves, respectively.

The role of the liquefiable bed(s) on the occurrence and type of SSDSs was further studied through relationships shown in Fig. 11e–f. In these graphs, the thickness of the liquefiable bed(s) was normalised by the total tephra thickness (Fig. 11e) and by the thickness of the upper silt bed (Fig. 11f). We observed from these graphs that type 1 and 2 (10–100-mm long) SSDSs formed only in tephra layers in which the thickness of liquefiable bed(s) was <45 % of the total tephra thickness (i.e., $h_{Def}/h_{Tot} < 0.45$) and up to two times thicker than the upper silt bed (i.e., $h_{Def}/h_{Silt} < 2$). This finding implies that the presence of a thick upper silt bed (in relation to the liquefiable beds) is an important control for the liquefaction process forming these two types of SSDSs in our study. Type 3 (<10-mm long) SSDSs, on the other hand, formed over a wider range of proportions of internal tephra beds (i.e., $0.2 < h_{Def}/h_{Tot} < 1.0$ and $1 < h_{Def}/h_{Silt} < 9$), indicating that the liquefaction process forming this type of SSDSs was driven to a lesser extent by the presence of an upper silt bed.

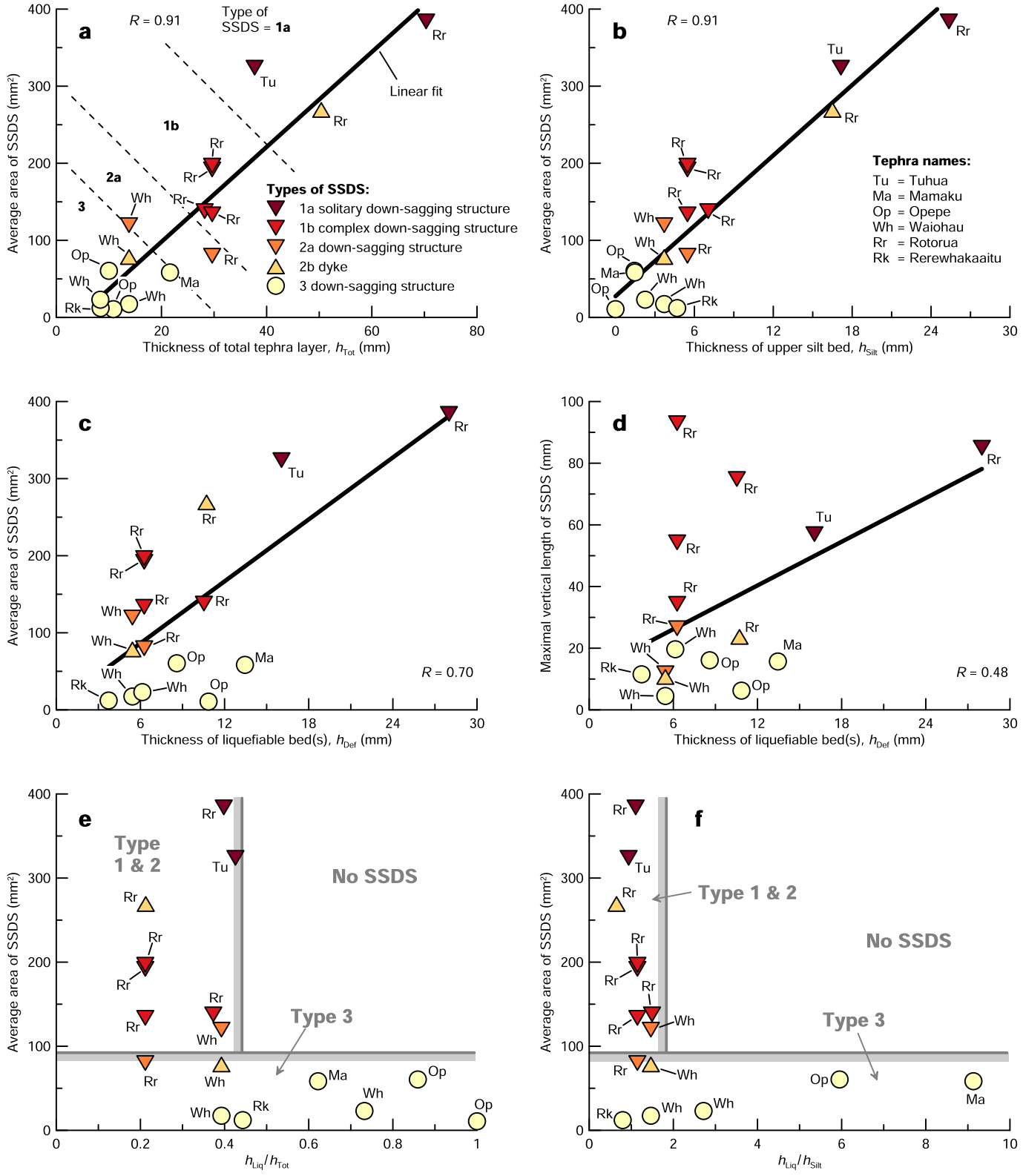

Fig. 11. Correlation between intact tephra and SSDS dimensions. (a–c) Correlations between average area of SSDSs and tephra thickness, specifically: (a) thickness of total tephra layer; (b) thickness of upper silt bed; and (c) thickness of liquefiable bed(s). (d) Correlation between thickness of liquefiable bed(s) and maximal vertical length of SSDSs. (e–f) Influence of proportions of liquefiable bed(s) on occurrence and type of SSDSs, with respect to (e) thickness of total tephra layer and (f) thickness of upper silt bed.

6.2.2. Down-sagging structures

The down-sagging structures reported in the present study exhibited internal flow structures and may resemble downward-directed dykes formed as consequence of fluidisation in the later stage of liquefaction (Owen et al., 2011). However, downward-directed dykes are physically impossible (even in reverse b–a density gradient systems) due to the normal hydraulic gradient in the pore water. The only exception for downward-directed dyke formation due to fluidisation is in

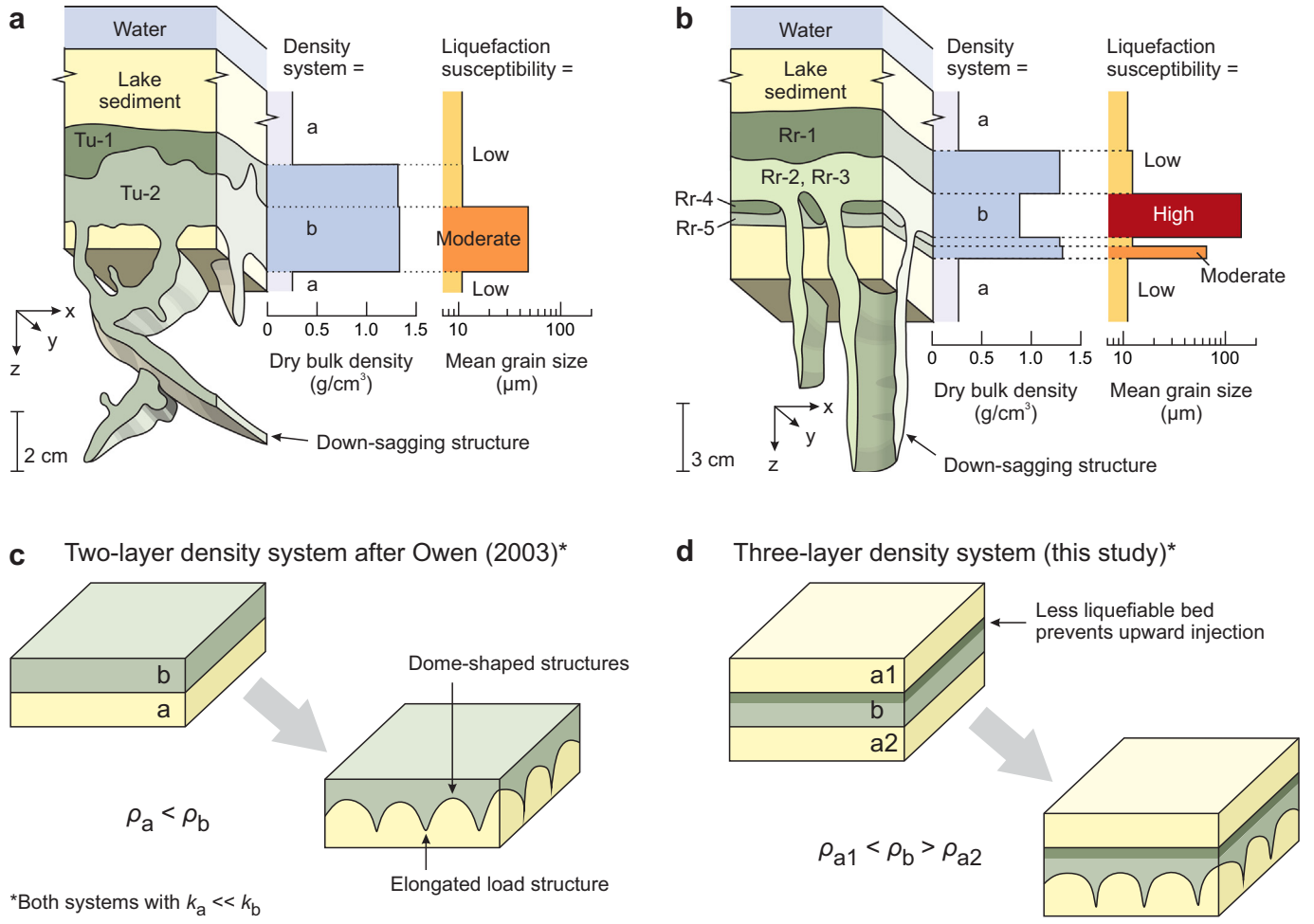

Fig. 12. Schematic illustrations of density systems in our study. (a–b) Variability in bulk dry density and mean grain size of organic lake sediments and internal beds of (a) Tuhua (Tu) and (b) Rotorua (Rr) tephras. Both tephras formed a–b–a density systems together with overlying and underlying organic lake sediment. The liquefiable internal tephra beds exhibited considerably higher mean grain sizes than organic lake sediments and upper silt beds, indicating higher degree of liquefaction susceptibilities. (c–d) Schematic diagrams showing the driving force of load structure formation for reverse density gradients that occur in (c) two-layer b–a density systems (after Owen, 2003) and (d) three-layer a–b–a density systems (this study). The two-layer density system is solely controlled by the reverse density contrast of the two layers, whereas in the three-layer density system, the less liquefiable upper silt bed prevented upward-directed dyke formation. The three-layer density system is considered a valid model for load structure formation (i.e., down-sagging structures) reported in our study. ρ and k denote the densities and relative kinematic viscosities of the reverse density system, respectively (Anketell et al., 1970).

subglacial environments, where the hydrogeological system may allow for injections being directed upwards, laterally, and downwards (Eyles and Clark, 1985). Downward-directed dykes are not feasible in our study because the northern North Island of New Zealand did not undergo significant glaciation (i.e., no glacierisation) before or since the formation of the lakes within the Hamilton lowlands (Newnham et al., 1989; Newnham et al., 1999; Barrell et al., 2013; Lorrey and Bostock, 2017).

Alternatively, the down-sagging structures could have formed as sand infills into fissures and cracks in environments controlled by extensional tectonics. This type of SSDSs is commonly referred to as Neptunian dyke and is considered to form passively due to gravity and not necessarily because of the process of fluidisation and liquefaction (Moretti and Sabato, 2007; Basilone et al., 2016). The Hamilton lowlands are not known to have been affected by any extensional tectonics in the past 20 kyrs (e.g., Edbrooke, 2005). Furthermore, it is considered unlikely here that fissures and cracks could form in the soft, unconsolidated, organic lake sediment. Therefore, it is not possible that the down-sagging structures reported in our study are Neptunian dykes.

We conclude that the down-sagging structures most closely represent some sort of load structures. The driving force of deformation of load structures is considered to be related to gravitational instabilities caused by the reverse density gradient system between the tephra layer and the relatively less-dense organic lake sediment below (Anketell et al., 1970). In our study, all types of down-sagging structures occurred in tephra deposits interlayered with organic lake sediment and commonly containing an upper silt bed.

To better understand the driving mechanism in such a system, dry bulk densities and mean grain sizes were obtained for the relevant internal beds of the Tuhua and Rotorua tephras, these being the two thickest tephra layers in our study. These parameters were plotted next to conceptual representations of those tephra layers once liquefied (Fig. 12a–b). The SSDSs shown in these conceptual three-dimensional models represent simplifications of the type 1a solitary down-sagging structures presented for Tuhua and Rotorua tephras in Fig. 6. Both Tuhua and Rotorua tephra layers exhibited dry bulk densities up to ~four times larger than those of the overlying and underlying organic lake sediment and, thus, created three-layer a–b–a density systems. Furthermore, the mean grain size $\bar{x}$ (here representing the position of the grain size distribution curve relative to the boundaries of liquefiable soils) was found to be considerably larger for the liquefiable beds ($60 \leq \bar{x} \leq 130$ μm) than for the organic lake sediments and upper silt beds (the last two having $\bar{x} \approx 10$ μm). Based on these grain size results, the liquefiable beds of Tuhua (Tu-2) and Rotorua (Rr-2, Rr-3) tephras are considered to have moderate (i.e., "potentially liquefiable", sensu Tsuchida, 1970) and high susceptibilities to liquefaction (i.e., "liquefiable", sensu Tsuchida,

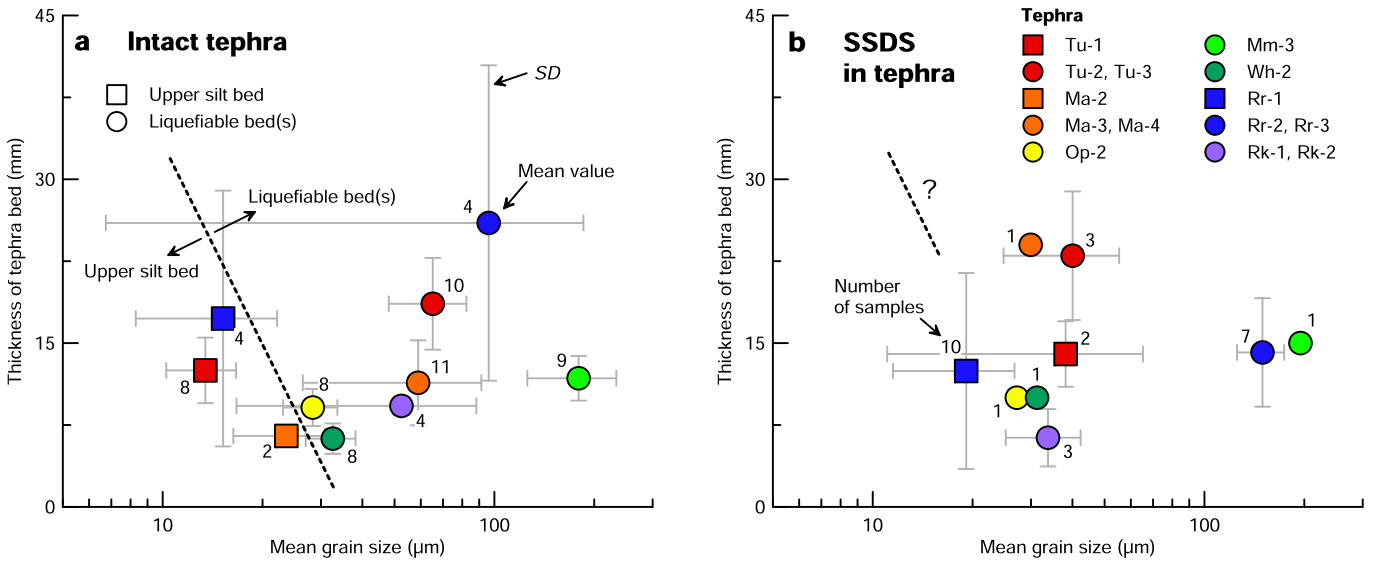

Fig. 13. Mean grain size and thickness of internal tephra beds of the seven major tephra layers compared between (a) intact tephra layers and (b) tephra layers that exhibited SSDSs. The influence of tephra properties on the liquefaction susceptibility can be considered negligible on the basis of available data. Note that a considerable number of tephras could not be included in the comparison because grain size data and internal bedding characteristics were not available for all cores. Dashed lines indicate a potential threshold between the tephra properties of the upper silt bed and the liquefiable beds. Abbreviated tephra names are given in full in Fig. 3a.

1970), respectively, whereas the organic lake sediment and upper silt beds may be considered to have low susceptibility to liquefaction.

Collecting dry bulk density samples from the other tephra samples was not feasible because of their thinness. The grain size distribution curves of the upper silt beds (where applicable), and of the liquefiable beds of the remaining tephra layers (i.e., Mamaku, Opepe, Mangamate, Waiohau, Rerewhakaaitu), followed similar trends as shown for Tuhua and Rotorua tephras (Fig. 10). Therefore, we conclude that the remaining tephras probably deformed because of a similar driving mechanism as that described for the Tuhua and Rotorua tephras.

Building on the early work of Anketell et al. (1970), Owen (2003) published comprehensive concepts for load structure formation in reverse b–a density systems. Hence, the morphologies of load structures depend on the contrast in density ρ and relative kinematic viscosity k between the upper and lower layer (Fig. 12c). For reverse b–a density systems (i.e., $\rho_a < \rho_b$), for which the relative kinematic viscosity of the lower layer is much smaller than that of the upper layer (i.e., $k_a \ll k_b$), it may be expected that narrow, elongated, downward-directed load structures comprising the relatively denser material, would form together with wide, upward-directed dome-shaped structures comprising the relatively less-dense material (Owen, 2003). The down-sagging structures we have reported here resemble the narrow, elongated load structures of this model.

We adapted the concept for load structure formation published by Owen (2003) to three-layer (a–b–a) density systems (Fig. 12d), where units a1 and a2 represent the organic lake sediment above and below unit b of relatively higher density (i.e., a tephra layer containing the upper silt bed). The organic lake sediment is assumed to exhibit a considerably lower kinematic viscosity than the tephra layer. The upper, less-dense unit a1 likely exhibits a slightly lower density and stress state than the underlying, less-dense unit a2, due to normal consolidation of the sediment column in the lake. Therefore, liquefaction in unit b would cause upward-directed intrusion into the overlying sediment unit a1. However, the presence of a less-liquefiable permeability barrier at the top of the central unit b is preventing upward-directed dyke formation. Instead, the tephra liquefies, resulting in loss of shear strength, and behaves in a viscous fluid-like manner, whilst sagging downwards into the underlying less-dense organic lake sediment. A similar driving force of deformation has been proposed for multi-layered reverse density systems (Moretti and Ronchi, 2011).

Wide, upward-directed, dome-shaped structures are commonly associated with this type of load structure (Owen, 2003). However, wide, upward-directed dome-shaped structures were not seen in our study. This is probably a result of the coring and sampling approach used in our study. The use of sediment/well cores to study large-scale SSDSs, which can vary in dimensions and type within relatively small lateral distances (Morsilli et al., 2020), has limitations, as discussed comprehensively by Ezquerro et al. (2015).

Törő and Pratt (2016) studied a lacustrine sedimentary record from the Eocene Green River Formation (Wyoming, U.S.A.) and reported small upward- and downward-directed SSDSs in three-layer a–b–a systems. It is considered likely here that the concept for load structure formation in three-layer (a–b–a) density systems of our study could be applicable to other lacustrine sedimentary records, such as the one studied by Törő and Pratt (2016).

6.2.3. Dykes

Dykes were observed only twice among the large number of down-sagging structures described in our study and were restricted to small intrusions from the liquefiable source beds into the upper less-liquefiable silt beds (Fig. 8). Such upward-directed injection follows the deformation mechanism for sand liquefaction in normal density gradients (Rodríguez-Pascua et al., 2000; Owen and Moretti, 2011; Belzyt et al., 2021).

6.2.4. Collapse structures

In the present study, we observed distinctive collapse structures, sometimes with associated faults, that coincided with the down-sagging structures (Figs. 6–9). Collapse structures were characterised by the mixing of overlying organic lake sediment with parts of the upper silt bed of the tephras, sometimes forming fold-like structures (e.g., Fig. 7a). Similar deformation structures have been interpreted as water-escape structures due to fluidisation following liquefaction in sandy beds that were constrained by less-permeable beds (Moretti and Sabato, 2007). Here, the collapse structures and associated faults are instead considered to have resulted from the collapse of organic lake sediment and the upper silt bed into voids created by the down-sagging of tephra material into underlying organic lake sediments.

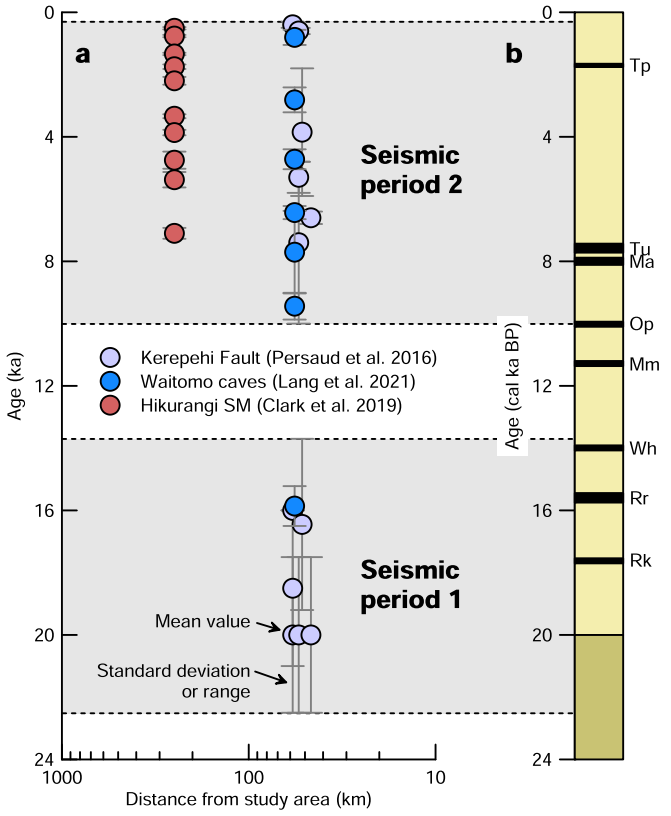

Fig. 14. Palaeoseismic activity in the surroundings of the Hamilton lowlands detected by means of fault rupture within the zone of Kerepehi and Te Puninga faults (located ~50 km northeast of the study area) (Persaud et al., 2016; Van Dissen et al., 2021), damage observed in the Waitomo caves (located ~57 km south of the study area) (Lang et al., 2021; Williams, 2021), and subduction earthquakes in the Hikurangi Subduction Margin (SM) (located ~250 km southeast of the study area) (Clark et al., 2019). The palaeoseismic activity clusters within two time periods, extending from 22.5 to 13.7 and 10.0 to 0.3 cal ka, respectively. The three oldest tephra layers (Rerewhakaitu, Rotorua, Waiohau) were deposited during the first seismic period, whereas the three youngest tephra layers (Opepe, Mamaku, Tuhua) were deposited during the second seismic period. Liquefaction in the three oldest tephra layers could have been triggered either by activity in the first or second seismic period, or both, whereas the three youngest tephra layers were likely triggered by activity in the second seismic period. Abbreviated tephra names are given in full in Fig. 3a.

6.3. Triggering mechanism

6.3.1. Non-seismic triggers

Liquefaction can be triggered by many different allochthonous processes (Owen and Moretti, 2011), such as pressure fluctuations due to water waves and turbulent water flow (e.g., Dzuynski and Smith, 1963; Okusa, 1985), tsunamis (e.g., Benson et al., 1997), tidal shear (e.g., Wells et al., 1980), rapid sediment loading (Anketell et al., 1970), groundwater seepage (e.g., Li et al., 1996), periglacial processes (Harris et al., 2002), and impacts of extra-terrestrial objects (Alvarez et al., 1998).

The lakes of our study occur in basins formed within sheltered embayments in the Hamilton lowlands with no connection to the ancestral Waikato River once formed because of the latter's subsequent entrenchment after ~17.5 cal ka BP (Newnham et al., 2003; Lowe and Green, 2023). Therefore, pressure fluctuations due to water waves and turbulent flow, tsunamis, and tidal shear are considered unlikely to be trigger mechanisms. Moreover, the tephras were deposited very rapidly, mantling the lake-bed morphology, a characteristic of tephra-fall deposition as noted earlier (Lowe, 1985; Lowe, 2011; Houghton and Carey, 2015). They were then buried by very slow deposition of organic lake sediments with typical sedimentation rates of ~0.1–0.5 mm/yr (Green and Lowe, 1985; Newnham et al., 1989), making it highly unlikely that overlying sediments caused significant excess pore pressure within tephra layers. Seepage has not been observed as a liquefaction trigger in lacustrine environments, and is known to produce predominantly tubular SSDSs (Li et al., 1996). In the present study, down-sagging structures were observed to be sheet-like rather than tubular (e.g., Fig. 6), excluding seepage as a potential triggering mechanism. There are no indications that impacts of extra-terrestrial objects or periglacial processes, played a role in triggering liquefaction in our study, and the northern North Island environment is too temperate for periglacial processes (e.g., Newnham et al., 1989; Newnham et al., 1999; Leathwick et al., 2003; Lorrey and Bostock, 2017).

6.3.2. Seismic trigger

A number of criteria are commonly used in order to assess the likelihood for seismic (autochthonous) triggers of SSDSs (Owen and Moretti, 2011). In recent earthquakes, liquefaction has been observed in wide areas around the epicentre (Cubrinovski et al., 2011). Seismically induced SSDSs should therefore be of large lateral and areal extent. In the present study, SSDSs were observed in nine out of ten lakes extending over a wide area (with a maximum extent of ~40 km) within the Hamilton lowlands (Figs. 1, 3). We acknowledge here that core records analysed in our study were not suitable to comprehensively assess the lateral extent of liquefaction because sediment cores can only reflect sedimentary successions at a single location (Ezquerro et al., 2015), but, nevertheless, we obtained multiple cores from lakes across the study area and, thus, providing a degree of replication from multiple locations (Table S1).

The effect of seismically-induced liquefaction on susceptible sediment is pervasive, which means that SSDSs should be laterally continuous, with some notable exceptions (Morsilli et al., 2020), unless there is some significant variation in sediment properties (Owen and Moretti, 2011). The present study found that internal bedding characteristics and grain size distribution of some tephra layers varied throughout the Hamilton lowlands (Figs. 4, 10). The influence of this variability on liquefaction susceptibility of these tephras was studied by comparing mean grain size and thicknesses of liquefiable beds and upper silt bed between tephra layers that resisted the triggering and stayed intact (i.e., no SSDSs observed) and those that liquefied (i.e., SSDSs observed) (Fig. 13). The available data of mean grain size and thickness of internal beds compiled in Fig. 13 exhibited a considerable scatter. However, the tephra properties of intact tephra layers were commonly within the standard deviation of those obtained for liquefied tephra layers, indicating variations in tephra properties were not a significant influence on whether or not liquefaction was triggered. Fig. 13 also highlights the fact that the deformation of tephra layers did not cause a significant change in thickness of tephra layers and their upper silt beds. We note that a considerable number of tephras could not be included in the comparison because detailed grain size data and internal bedding characteristics were not available for all cores. Interestingly, Fig. 13a could also be used to differentiate the bedding characteristics of upper silt beds and liquefiable beds of intact tephra layers (dashed line in Fig. 13a).

The pervasive nature of SSDSs could be observed in the 1b complex down-sagging structures because deformation in the associated tephra layers was not restricted to a single SSDS per core. Other types of SSDSs, especially the type 2 down-sagging structures and dykes, are considered less pervasive as only single SSDSs were observed in each core. This observation may have been influenced by the use of sediment cores, being only 50 to 80 mm wide, rather than natural outcrops (Ezquerro et al., 2015) (which do not exist). However, it may be concluded here that the presence of at least one type of pervasive SSDS, the type 1b complex down-sagging structure, is a sufficient indication for a seismic trigger of all SSDSs because the different types of SSDSs occurred in the same tephra layers within the same sedimentary successions.

Earthquakes are recurring events (Owen and Moretti, 2011). Therefore, seismically induced SSDSs should be repeated throughout a

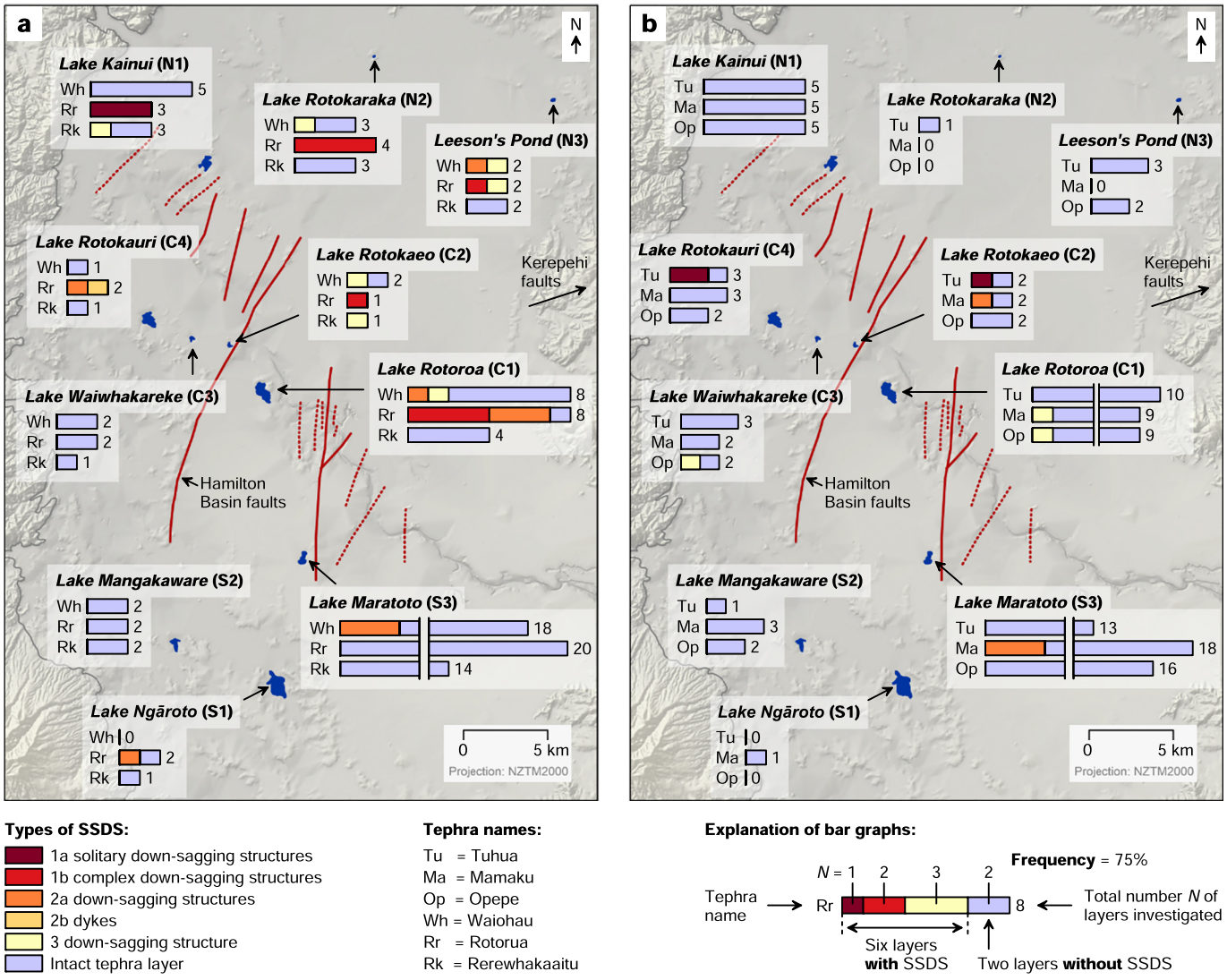

Fig. 15. Spatial and temporal analysis of SSDSs observed in the ten lakes within the Hamilton lowlands. Type and frequency of SSDS occurrence for (a) the older tephra layers (i.e., Rerewhakaitu, Rotorua, Waiohau), deposited between 17.5 and 14.0 cal ka BP, and (b) the younger tephra layers (i.e., Opepe, Mamaku, Tuhua), deposited between 10.0 and 7.6 cal ka BP.

vertical sedimentary succession. In our study, SSDSs were reported for the seven major tephra layers deposited between 17.5 and 7.6 cal ka BP. Timing of triggering is difficult to obtain, however, because the organic lake sediment and tephra layers are considered to be essentially unconsolidated with minor or no ageing effects having taken place since deposition. One or more triggering events may have caused liquefaction in the lakes within the Hamilton lowlands. Subsequent events may have caused re-liquefaction, although this is often considered a rare phenomenon (Obermeier, 1996; Owen and Moretti, 2011). Therefore, the repeated occurrence of SSDSs could not be used as a valid criterion to assess seismic triggering in the present study.

Morphological similarities between SSDSs and structures formed by liquefaction in recent earthquakes might seem a valuable criterion for recognising a seismic origin (Owen and Moretti, 2011). The load structures and dykes reported in our study resembled liquefaction structures that have been unambiguously linked with seismic triggering (Rodríguez-Pascua et al., 2000).

The proximity of faults that have been active during the formation of SSDSs, and which have the potential to have caused moment magnitude $M > 5$ earthquakes (Rodríguez-Pascua et al., 2000), is considered as strong evidence for the seismically-induced triggering of liquefaction (Owen and Moretti, 2011). A number of faults may have been active since the deposition of the first major tephra layer (Fig. 14). Large (moment magnitude $M > 7.2$) palaeoearthquakes occurred between 7.3 and 0.5 cal ka BP at the offshore subduction margin, the Hikurangi Trough located ~250 km to the southeast of our study area (Fig. 1b) (Clark et al., 2019). At least three of the earthquakes that occurred at the Hikurangi Trough since the deposition of the tephra layers in the Hamilton lowlands originated from ruptures longer than 450 km along the margin (Clark et al., 2019). Assuming a fault width of 150 km and using the new fault scaling relationship from the National Hazards Model 2022 for New Zealand (Gerstenberger et al., 2022), we calculated moment magnitudes of $8.4 \leq M \leq 8.9$ for the three events. From global and New Zealand-specific liquefaction observations (Maurer et al., 2015), the maximal distance from a M-8.9 rupture at which liquefaction can occur is somewhere between 150 and 250 km. We note that in order for earthquake waves originating from faulting within the Hikurangi Trough to reach the Hamilton lowlands, they must travel through the Taupō Volcanic Zone, the deposits in which are known to attenuate seismic waves (McVerry et al., 2006). Thus, the actual maximal distance at which liquefaction can occur may be considerably smaller. Nevertheless, we conclude here that there is still a potential for faulting within the Hikurangi Trough to have caused liquefaction within the Hamilton lowlands, despite attenuation of seismic waves within the Taupō Volcanic Zone.

Two periods of seismic activity were inferred from palaeoseismic mapping at the Kerepehi and Te Puninga faults located within the Hauraki plains up to ~46 to ~58 km to the northeast (Fig. 1b), and from fault activity observations and damage mapped in the Waitomo Caves, located ~57 km to the south (Persaud et al., 2016; Lang et al., 2021; Van Dissen et al., 2021; Williams, 2021; Villamor, 2022) (Fig. 14). The Kerepehi and Te Puninga faults were estimated to have caused large ($M = 7$) earthquakes (Persaud et al., 2016; Villamor, 2022). Ground motion simulations of an *M*-7 earthquake at the Kerepehi Fault yielded peak ground accelerations between 0.15 and 0.27 g at the lakes of the present study (Dempsey et al., 2021), well above the minimum peak ground acceleration of 0.07 g needed to cause liquefaction in sandy soils of New Zealand (Maurer et al., 2015). However, the liquefaction threshold of Maurer et al. (2015) should be applied with care here because it does not encompass the liquefaction of pumiceous tephra-derived soils, which in some cases have been found to exhibit considerably higher liquefaction resistance than sandy (non-pumiceous) soils (Asadi et al., 2018).

The two periods of seismic activity identified for the Hauraki Plains align well with the time of deposition of six of the seven major tephra layers (Fig. 14). The first seismic period (~22.3 to ~13.7 cal ka BP) encompasses deposition of the three oldest tephra layers (i.e., Rerewhakaaitu, Rotorua, and Waiohau), whereas the second seismic period (~10.0 to ~0.3 cal ka BP) encompasses deposition of the three youngest tephra layers (i.e., Opepe, Mamaku, Tuhua). It may be concluded here that fault activity at the Kerepehi and/or Te Puninga faults is a plausible seismic trigger for liquefaction that caused SSDSs in our study.

Some aspects of the frequency or complexity of SSDSs in our study were found to decrease with distance from a fault that may have been active during the deformation process, which is considered to be the strongest evidence for the seismic triggering of SSDSs (Pope et al., 1997; Owen and Moretti, 2011). A potential zonation of SSDSs within the Hamilton lowlands was assessed spatially and temporarily through Fig. 15. For two time periods, reflecting the deposition of the three oldest tephras (i.e., Rerewhakaaitu, Rotorua, Waiohau) and the three youngest tephras (i.e., Opepe, Mamaku, Tuhua), respectively, the number of each type of SSDSs was plotted, for each lake, in relation to the total number of cores in which a particular tephra layer could be observed (i.e., was present and not classified as discontinuous). For example, in Lake Rotoroa (C1), the total number of SSDSs observed for Waiohau tephra was two (i.e., one type 2a down-sagging structure and one type 3 down-sagging structure). The total number of Waiohau tephra layers assessed at this lake (i.e., classified as intact or showing signs of SSDSs) was eight. Dividing the number of SSDSs by the number of total tephra layers assessed yielded a frequency estimate for SSDS occurrence for a particular lake (being 25 % in this particular example). The total number of observations varied between lakes, affecting the confidence of the presented analysis. For example, at Lake Ngāroto the total number of tephra layers analysed was relatively low, providing some uncertainty when obtaining a frequency of SSDS occurrence. In contrast, at Lake Maratoto, where around 30 sediment cores were taken (Green and Lowe, 1985), the total number of tephra layers being analysed ranged from 13 to 20 between different tephras, providing higher certainty when calculating the frequency of SSDS occurrence.

When considering the three oldest tephra layers (Fig. 15a), the complexity (i.e., type 1–3 SSDSs exhibit descending degree of complexity) and frequency of SSDSs increased consistently towards the northeast, suggesting a link between seismic activity on the Kerepehi and/or Te Puninga faults and liquefaction in the Hamilton lowlands. We acknowledge that the trend in complexity of SSDSs could be partly the result of variability in tephra thickness as discussed earlier (see Fig. 11). However, a clear connection between tephra thickness variability (Fig. 4) and complexity of SSDSs (Fig. 15) could not be found. The trend in complexity towards the northeast could not be observed for the three youngest tephra layers (Fig. 15b). For these layers, the occurrence of SSDSs was instead restricted to the central part of the study area, with the complexity and frequency of SSDSs being lower than that for the older tephra layers. The occurrence of SSDSs within the younger tephra layers matches the location of the recently-mapped Hamilton Basin faults (Moon and de Lange, 2017; Van Dissen et al., 2021). The Hamilton Basin faults occur in the upper Hamilton Ash beds, dated at ~74 ka BP (Lowe, 2019). Hence, the Hamilton Basin faults are currently considered older than the tephra layers analysed in the present study, because the riverine and riverine-phytogenic lakes in which these occur were formed by deposition of the ~20-ka-BP-old Hinuera Formation (Kear and Schofield, 1978; Lowe and Green, 1992; McCraw, 2011). It is currently unknown if the Hamilton Basin faults were active after the deposition of the Hinuera Formation. However, from the spatial proximity of the SSDSs in the younger tephra layers to the Hamilton Basin faults, we infer that they may have been triggered by a near-field seismic source within the Hamilton lowlands, therefore potentially from one or more of the Hamilton Basin faults. Alternatively, liquefaction in the younger tephra layers could have been triggered by far-field earthquakes from the offshore Hikurangi subduction margin.

7. Conclusions

The present study analysed a large number of soft-sediment deformation structures (SSDSs) that occurred in seven unconsolidated, up to 8-cm thick, silicic tephra layers that were deposited in ~35 riverine and riverine-phytogenic lakes within the Hamilton lowlands, central North Island, New Zealand, since 17.5 cal ka BP. Based on sediment descriptions, X-ray computed tomography (CT) scanning, and analyses of dry bulk density, grain size distribution, and Atterberg limits of samples from cores taken from ten lakes, the following conclusions are made.

- SSDSs were classified into elongated load structures (i.e., down-sagging structures) of different dimensions, ranging from millimetre- to decimetre-scale, and centimetre-long dykes.
- Deformations commonly involved the intrusion of very fine sand to medium sand internal tephra beds into underlying organic lake sediments. Tephra layers commonly exhibited an upper silt bed, which was not directly involved in the deformation process.
- The organic lake sediment and the upper silt bed are considered as less liquefiable, whereas the very fine sand to medium sand internal tephra beds are considered as liquefiable.
- The dimensions of SSDSs linearly increased with the thickness of the source tephra layer.
- The tephra layers, and the organic lake sediments above and below them, form three-layer (a–b–a) density systems. It is inferred here that downward-directed deformation was favoured by this three-layer (a–b–a) density system, together with the presence of an upper, less-liquefiable silt bed preventing upward intrusion during the liquefaction process.
- The spatial and temporal occurrence of SSDSs within the Hamilton lowlands provided some evidence that liquefaction of the older tephras, deposited between 17.5 and 14 cal ka BP, was triggered by a seismic source to the northeast (i.e., Kerepehi and/or Te Puninga faults in the adjacent Hauraki Plains).
- Liquefaction of the younger tephra layers, deposited between 10.0 and 7.6 cal ka BP, may have been triggered by local faults within the Hamilton lowlands, namely one or more of the Hamilton Basin faults, or by distant faulting at the Hikurangi subduction margin.

Supplementary data to this article can be found online at https://doi.org/10.1016/j.sedgeo.2022.106327.

Data availability

Data will be made available on request.

Declaration of competing interest

The authors declare that they have no known competing financial interests or personal relationships that could have appeared to influence the work reported in this paper.

Acknowledgments

We thank iwi of Ngāti Wairere (especially Mrs Hekeiterangi Broadhurst and Wiremu Puke) and Ngā Iwi Tōpū O Waipā, Zeke Fiske and Hamilton City Council, Tony Roxburgh and Waipā District Council, the Department of Conservation, and private land owners for their ongoing support in providing access to lakes for coring and in other ways. Marcus Vandergoes, Susie Wood, Andrew Rees, and Henry Gard, representing the Lakes380 project, are thanked for sediment coring in 2020 and 2022 (Vandergoes and Rees also undertook coring in 2016), Phillip Hassall from Hamilton Radiology for supporting core CT scanning, Alex Harpur for helping to describe sediment cores in 2016, Vittoria Gibbons for laboratory assistance, and Simon Lovatt and Carol Robinson for administrative support relating to funding. The paper is an output of the Commission on Tephrochronology (COT) of the International Association of Volcanism and Chemistry of the Earth's Interior (IAVCEI). We thank Massimo Moretti and an anonymous referee for their constructive comments on our paper.

MOK, DJL, VGM, JC, TI, PV, RAM, and RPO were supported by an MBIE Endeavour Fund (Smart Ideas) project "Evaluating earthquake risk using liquefied volcanic-ash layers in lakes" (contract UOWX1903). MOK, DJL, VGM, JC, TI, and PV were supported by the Marsden Fund project "Earth-shaking insight from liquefied volcanic-ash (tephra) layers in lakes: using geotechnical experiments, CT-scanned lake sediment cores, and tephrochronology to map and date prehistoric earthquakes" (contract UOW1902). DJL and RCL were supported by an Earthquake Commission (EQC) project "Hidden hazards: revealing volcanic ashfall hazards in the Waikato region by detecting and analysing cryptotephras in sediments" (contract 15/U713). PV and DJL were supported by an Earthquake Commission (EQC) project "Paleoseismology of the newly discovered Te Puninga Fault, Hauraki Plains" (contract BIG 012 2020). DJL and RCL were supported by a University of Waikato SIF Research Grant (2016) "Tephra seismites: a new tool to evaluate, date, and map paleoseismicity using tephra liquefaction in lake sediments". RCL was supported by a PhD fees-scholarship, funded by Waikato Regional Council. PV was supported by an MBIE Strategic Science Investment Fund (GNS-Hazards and Risk Management Programme). RPO was supported by the NZ Centre for Earthquake Resilience (QuakeCoRE). RJ was supported by an AIM Facility fund in part from the UK's Engineering and Physical Sciences Research Council (EP/M028267/1).

References

Alloway, B.V., Lowe, D.J., Larsen, G., Shane, P.A.R., Westgate, J.A., 2013. Tephrochronology. In: Elias, S., Mock, C. (Eds.), The Encyclopaedia of Quaternary Science, 2nd edition Elsevier, Amsterdam, pp. 277–304.

Alvarez, W., Staley, E., O'Connor, D., Chan, M.A., 1998. Synsedimentary deformation in the Jurassic of southeastern Utah—a case of impact shaking? Geology 26, 579–582.

Anketell, J.M., Cegła, J., Dżułyński, S., 1970. On the deformational structures in systems with reversed density gradients. Annales. Societatis Geologorum Poloniae 40, 3–30.

Asadi, M.S., Asadi, M.B., Orense, R.P., Pender, M.J., 2018. Undrained cyclic behavior of reconstituted natural pumiceous sands. Journal of Geotechnical and Geoenvironmental Engineering 144, 04018045. https://doi.org/10.1061/(ASCE)GT.1943-5606.0001912.

ASTM D 4318-17e1, 2017. Standard Test Methods for Liquid Limit, Plastic Limit, and Plasticity Index of Soils. ASTM International https://doi.org/10.1520/D4318-17E01.

ASTM D2487-06, 2010. Standard Practice for Classification of Soils for Engineering Purposes (Unified Soil Classification System). ASTM International https://doi.org/10.1520/D2487-06.

ASTM D7348-21, 2021. Standard Test Methods for Loss on Ignition (LOI) of Solid Combustion Residues. ASTM International https://doi.org/10.1520/D7348-21.

Barrell, D.J.A., Almond, P.C., Vandergoes, M.J., Lowe, D.J., Newnham, R.M., NZ-INTIMATE members, 2013. A composite pollen-based stratotype for inter-regional evaluation of climatic events in New Zealand over the past 30,000 years (NZ-INTIMATE project). Quaternary Science Reviews 74, 4–20. https://doi.org/10.1016/j.quascirev.2013.04.002.

Basilone, L., Sulli, A., Morticelli, M.G., 2016. The relationships between soft-sediment deformation structures and synsedimentary extensional tectonics in Upper Triassic deep-water carbonate succession (Southern Tethyan rifted continental margin—Central Sicily). Sedimentary Geology 344, 310–322. https://doi.org/10.1016/j.sedgeo.2016.01.010.

Bektas, O., Çapkinoglu, S., Akdag, K., 2001. Successive extensional tectonic regimes during the Mesozoic as evidenced by neptunian dikes in the Pontide Magmatic Arc, Northeast Turkey. International Geology Review 43, 840–849. https://doi.org/10.1080/00206810109465051.

Belzyt, S., Pisarska-Jamroży, M., Bitinas, A., Woronko, B., Phillips, E.R., Piotrowski, J.A., Jusienė, A., 2021. Repetitive Late Pleistocene soft-sediment deformation by seismicity-induced liquefaction in north-western Lithuania. Sedimentology 68, 3033–3056. https://doi.org/10.1111/sed.12883.

Benson, B.E., Grimm, K.A., Clague, J.J., 1997. Tsunami deposits beneath tidal marshes on northwestern Vancouver Island, British Columbia. Quaternary Research 48, 192–204. https://doi.org/10.1006/qres.1997.1911.

Blott, S.J., Pye, K., 2001. GRADISTAT: a grain size distribution and statistics package for the analysis of unconsolidated sediments. Earth Surface Processes and Landforms 26, 1237–1248. https://doi.org/10.1002/esp.261.

Boulanger, R.W., Idriss, I.M., 2006. Liquefaction susceptibility criteria for silts and clays. Journal of Geotechnical and Geoenvironmental Engineering 132, 1413–1426. https://doi.org/10.1061/(ASCE)1090-0241(2006)132:11(1413).

Brlek, M., Kutterolf, S., Gaynor, S., Kuiper, K., Belak, M., Brčić, V., ... Schaltegger, U., 2020. Miocene syn-rift evolution of the North Croatian Basin (Carpathian–Pannonian Region): new constraints from Mts. Kalnik and Požeška gora volcaniclastic record with regional implications. International Journal of Earth Sciences 109 (8), 2775–2800.

Churchman, G.J., Lowe, D.J., 2012. Alteration, formation, and occurrence of minerals in soils. In: Huang, P.M., Li, Y., Sumner, M.E. (Eds.), Handbook of Soil Sciences. Properties and Processes, 2nd edition CRC Press, USA, pp. 20.21–20.72.

Clark, K., Howarth, J., Litchfield, N., Cochran, U., Turnbull, J., Dowling, L., Howell, A., Berryman, K., Wolfe, F., 2019. Geological evidence for past large earthquakes and tsunamis along the Hikurangi subduction margin, New Zealand. Marine Geology 412, 139–172. https://doi.org/10.1016/j.margeo.2019.03.004.

Cubrinovski, M., Bradley, B., Wotherspoon, L., Green, R., Bray, J., Wood, C., Pender, M., Allen, J., Bradshaw, A., Rix, G., 2011. Geotechnical aspects of the 22 February 2011 Christchurch earthquake. Bulletin of the New Zealand Society for Earthquake Engineering 44, 205–226. https://doi.org/10.5459/bnzsee.44.4.205-226.

Cubrinovski, M., Bray, J.D., De La Torre, C., Olsen, M.J., Bradley, B.A., Chiaro, G., Stocks, E., Wotherspoon, L., 2017. Liquefaction effects and associated damages observed at the Wellington CentrePort from the 2016 Kaikoura earthquake. Bulletin of the New Zealand Society for Earthquake Engineering 50, 152–173. https://doi.org/10.5459/bnzsee.50.2.152-173.

Dempsey, D., Eccles, J.D., Huang, J., Jeong, S., Nicolin, E., Stolte, A., Wotherspoon, L., Bradley, B.A., 2021. Ground motion simulation of hypothetical earthquakes in the upper North Island of New Zealand. New Zealand Journal of Geology and Geophysics 64, 570–588. https://doi.org/10.1080/00288306.2020.1842469.

Di Capua, A., De Rosa, R., Kereszturi, G., Le Pera, E., Rosi, M., Watt, S.F.L., 2022. Volcanically derived deposits and sequences: a unified terminological scheme for application in modern and ancient environments. Geological Society, London, Special Publications 520, 1–25. https://doi.org/10.1144/SP520-2021-201.

DIN 18126, 1996. Soil, investigation and testing - determination of density of non-cohesive soils for maximum and minimum compactness. Deutsches Institut für Normen e. V. https://doi.org/10.31030/7209583.

Dzuynski, S., Smith, A.J., 1963. Convolute lamination, its origin, preservation, and directional significance. Journal of Sedimentary Research 33, 616–627. https://doi.org/10.1306/74D70ED4-2B21-11D7-8648000102C1865D.

Edbrooke, S.W., 2005. Geology of the Waikato area. Institute of Geological and Nuclear Sciences 1:250,000 Geological Map 4. 1 sheet and 68p. IGNS, Lower Hut, 0478098774.

El Taki, H., Pratt, B.R., 2012. Syndepositional tectonic activity in an epicontinental basin revealed by deformation of subaqueous carbonate laminites and evaporites: seismites in Red River strata (Upper Ordovician) of southern Saskatchewan, Canada. Bulletin of Canadian Petroleum Geology 60, 37–58. https://doi.org/10.2113/gscpgbull.60.1.37.

Eyles, N., Clark, B.M., 1985. Gravity-induced soft-sediment deformation in glaciomarine sequences of the Upper Proterozoic Port Askaig Formation, Scotland. Sedimentology 32, 789–814. https://doi.org/10.1111/j.1365-3091.1985.tb00734.x.

Ezquerro, L., Moretti, M., Liesa, C.L., Luzón, A., Simón, J.L., 2015. Seismites from a well core of palustrine deposits as a tool for reconstructing the palaeoseismic history of a fault. Tectonophysics 655, 191–205. https://doi.org/10.1016/j.tecto.2015.05.025.

Folk, R.L., 1980. Petrology of Sedimentary Rocks. Hemphill Publishing Company, Austin, Texas (190 pp.).

Fortuin, A.R., Dabrio, C.J., 2008. Evidence for Late Messinian seismites, Nijar Basin, southeast Spain. Sedimentology 55, 1595–1622. https://doi.org/10.1111/j.1365-3091.2008.00959.x.

Froggatt, P.C., Lowe, D.J., 1990. A review of late Quaternary silicic and some other tephra formations from New Zealand: their stratigraphy, nomenclature, distribution, volume, and age. New Zealand Journal of Geology and Geophysics 33, 89–109. https://doi.org/10.1080/00288306.1990.10427576.

Gavrilov, Y.O., 2017. Reflection of seismic paleoevents in Mesozoic–Cenozoic terrigenous sequences of the northern Caucasus. Lithology and Mineral Resources 52, 1–19. https://doi.org/10.1134/S0024490217010035.

Gerstenberger, M.C., Bora, S., Bradley, B.A., DiCaprio, C., Van Dissen, R.J., Atkinson, G.M., Chamberlain, C., Christophersen, A., Clark, K.J., Coffey, G.L., et al., 2022. New Zealand National Seismic Hazard Model 2022 Revision: Model, Hazard and Process Overview. GNS Science.

Gladkov, A.S., Lobova, E.U., Deev, E.V., Korzhenkov, A.M., Mazeika, J.V., Abdieva, S.V., Rogozhin, E.A., Rodkin, M.V., Fortuna, A.B., Charimov, T.A., 2016. Earthquake-induced soft-sediment deformation structures in Late Pleistocene lacustrine deposits of Issyk-Kul lake (Kyrgyzstan). Sedimentary Geology 344, 112–122. https://doi.org/10.1016/j.sedgeo.2016.06.019.

Green, J.D., Lowe, D.J., 1985. Stratigraphy and development of c. 17 000 year old Lake Maratoto, North Island, New Zealand, with some inferences about postglacial climatic change. New Zealand Journal of Geology and Geophysics 28, 675–699. https://doi.org/10.1080/00288306.1985.10422541.

Green, J.D., Lowe, D.J., 1994. Origins and development. In: Clayton, J., de Winton, M. (Eds.), Lake Rotoroa: Change in an Urban Lake. National Institute of Water and Atmospheric Research Ecosystems Publication, Wellington, NZ, pp. 13–23.

Harris, C., Murton, J., Davies, M.C.R., 2002. Soft-sediment deformation during thawing of ice-rich frozen soils: results of scaled centrifuge modelling experiments. Sedimentology 47, 687–700. https://doi.org/10.1046/j.1365-3091.2000.00322.x.

Hodder, A.P.W., de Lange, P.J., Lowe, D.J., 1991. Dissolution and depletion of ferromagnesian minerals from Holocene tephras in an acid bog, New Zealand, and implications for tephra correlation. Journal of Quaternary Science 6, 195–208. https://doi.org/10.1002/jqs.3390060303.

Hodder, A.P.W., Naish, T.R., Lowe, D.J., 1996. Towards an understanding of thermodynamic and kinetic controls on the formation of clay minerals from volcanic glass under various environmental conditions. In: Pandalai, S.G. (Ed.), Recent Research Developments in Chemical Geology. Research Signpost, Trivandrum, India, pp. 1–11.

Hopkins, J.L., Millet, M.-A., Timm, C., Wilson, C.J.N., Leonard, G.S., Palin, M.J., Neil, H., 2015. Tools and techniques for developing tephra stratigraphies in lake cores: a case study from the basaltic Auckland Volcanic Field, New Zealand. Quaternary Science Reviews 123, 58–75. https://doi.org/10.1016/j.quascirev.2015.06.014.

Hopkins, J.L., Lowe, D.J., Horrocks, J.H., 2021. Tephrochronology in Aotearoa New Zealand. New Zealand Journal of Geology and Geophysics 64, 153–200. https://doi.org/10.1080/00288306.2021.1908368.

Houghton, B.F., Carey, R.J., 2015. Pyroclastic fall deposits. In: Sigurdsson, H. (Ed.), The Encyclopaedia of Volcanoes, second edition Elsevier, San Diego, pp. 599–616.

Hume, T.M., Sherwood, A.M., Nelson, C.S., 1975. Alluvial sedimentology of the Upper Pleistocene Hinuera Formation, Hamilton Basin, New Zealand. Journal of the Royal Society of New Zealand 5, 421–462. https://doi.org/10.1080/03036758.1975.10419362.

Ishihara, K., 1985. Stability of natural deposits during earthquakes. 11th International Conference on Soil Mechanics and Foundation Engineering. International Society for Soil Mechanics and Geotechnical Engineering, pp. 321–376.

Juvigné, E.T., Porter, S.C., 1985. Mineralogical variations within two widespread Holocene tephra layers from Cascade Range volcanoes, U.S.A. Géographie Physique et Quaternaire 39, 7–12.

Kang, H.C., Paik, I.S., Lee, H.I., Lee, J.E., Chun, J.H., 2010. Soft-sediment deformation structures in Cretaceous non-marine deposits of southeastern Gyeongsang Basin, Korea: occurrences and origin. Island Arc 19, 628–646. https://doi.org/10.1111/j.1440-1738.2010.00738.x.

Kear, D., Schofield, J.C., 1978. Geology of the Ngaruawahia subdivision. New Zealand Geological Survey Bulletin 88, 1–168.

Kirkman, J.H., McHardy, W.J., 1980. A comparative study of the morphology, chemical composition and weathering of rhyolitic and andesitic glass. Clay Minerals 15, 165–173. https://doi.org/10.1180/claymin.1980.015.2.07.

Kleyburg, M.A., Moon, V.G., Lowe, D.J., Nelson, C.S., 2015. Paleoliquefaction in Late Pleistocene alluvial sediments in Hauraki and Hamilton basins, and implications for paleoseismicity. Proceedings of 12th Australia New Zealand Conference on Geomechanics (ANZ 2015). NZ Geotechnical Society , pp. 524–531. https://hdl.handle.net/10289/9952.

Kramer, S.L., 1996. Geotechnical Eartqhuake Engineering. Prentice Hall, New Jersey (653 pp.).

Krumbein, W.C., Pettijohn, F.J., 1938. Manual of sedimentary petrography. Geologiska Föreningen i Stockholm Förhandlingar 61, 225–227. https://doi.org/10.1080/11035893909452786.

Lang, J., Baker, J., Williams, P., Rowland, J., Clark, K., Howarth, J., Hellstrom, J., Cross, T., Goded, T., 2021. Macro-characterisation of cave damage for palaeoseismological investigations in regions of low strain: a case study from central–western North Island (Waitomo caves), New Zealand. Quaternary Science Reviews 272, 107202. https://doi.org/10.1016/j.quascirev.2021.107202.

Langridge, R.M., Ries, W.F., Litchfield, N.J., Villamor, P., Van Dissen, R.J., Barrell, D.J.A., Rattenbury, M.S., Heron, D.W., Haubrock, S., Townsend, D.B., 2016. The New Zealand active faults database. New Zealand Journal of Geology and Geophysics 59, 86–96. https://doi.org/10.1080/00288306.2015.1112818.

Leathwick, J., Wilson, G., Rutledge, D., Wardle, P., Morgan, F., Johnston, K., McLeod, M., Kirkpatrick, R., 2003. Land Environments of New Zealand. Bateman, Auckland (184 pp.).

Leonard, G.J., Begg, J.G., Wilson, C.J.N., 2010. Geology of the Rotorua area: scale 1:250,000. Institute of Geological and Nuclear Sciences 1:250,000 Geological Map 5. 1 Sheet and 99p. IGNS, Lower Hutt.

Li, Y., Craven, J., Schweig, E.S., Obermeier, S.F., 1996. Sand boils induced by the 1993 Mississippi River flood: could they one day be misinterpreted as earthquake-induced liquefaction? Geology 24, 171–174.

Limaye, A., 2012. Drishti: a volume exploration and presentation tool. Developments in X-ray Tomography VIII. International Society for Optics and Photonics 85060X.

Loame, R.C., Lowe, D.J., Pittari, A., Davies, S.M., Magill, C.R., Vandergoes, M.J., Rees, A.B.H., Ross, N., 2018. Using CT scanning for reconnaissance and detection of cryptotephras in ~22,000-yr-old lake sediments, central Waikato region, New Zealand. Book of Abstracts, Crossing New Frontiers: INTAV International Field Conference on Tephrochronology, 'Tephra Hunt in Transylvania , pp. 41–42. https://iris.waikato.ac.nz/viewobject.html?cid=1&id=225746.

Lorrey, A.M., Bostock, H., 2017. The climate of New Zealand through the Quaternary. In: Shulmeister, J. (Ed.), Landscape and Quaternary Environmental Change in New Zealand. Atlantis Advances in Quaternary Sciencevol. 3. Atlantis Press, Paris, pp. 67–139.

Lowe, D.J., 1985. Application of impulse radar to continuous profiling of tephra-bearing lake sediments and peats: an initial evaluation. New Zealand Journal of Geology and Geophysics 28, 667–674. https://doi.org/10.1080/00288306.1985.10422540.

Lowe, D.J., 1988a. Late Quaternary volcanism in New Zealand: towards an integrated record using distal airfall tephras in lakes and bogs. Journal of Quaternary Science 3, 111–120. https://doi.org/10.1002/jqs.3390030202.

Lowe, D.J., 1988b. Stratigraphy, age, composition, and correlation of late Quaternary tephras interbedded with organic sediments in Waikato lakes, North Island, New Zealand. New Zealand Journal of Geology and Geophysics 31, 125–165. https://doi.org/10.1080/00288306.1988.10417765.

Lowe, D.J., 2011. Tephrochronology and its application: a review. Quaternary Geochronology 6, 107–153. https://doi.org/10.1016/j.quageo.2010.08.003.

Lowe, D.J., 2019. Using soil stratigraphy and tephrochronology to understand the origin, age, and classification of a unique Late Quaternary tephra-derived Ultisol in Aotearoa New Zealand. Quaternary 2, 1–34. https://doi.org/10.3390/quat2010009.

Lowe, D.J., Green, J.D., 1992. Lakes. In: Soons, J.M., Selby, M.J. (Eds.), Landforms of New Zealand, second edition Longman Paul, Auckland, pp. 107–143.

Lowe, D.J., Green, J.D., 2023. Origin and ages of Waikato lakes. In: Ozkundakci, D., Grainger, N., Dean-Speirs, T. (Eds.), Hidden Gems of the Waikato – The history, ecology and management of Waikato lakes. Waikato Regional Council, Hamilton (in press).

Lowe, D.J., Blaauw, M., Hogg, A.G., Newnham, R.M., 2013. Ages of 24 widespread tephras erupted since 30,000 years ago in New Zealand, with re-evaluation of the timing and palaeoclimatic implications of the Lateglacial cool episode recorded at Kaipo bog. Quaternary Science Reviews 74, 170–194. https://doi.org/10.1016/j.quascirev.2012.11.022.

Lowe, D.J., Rees, A.B.H., Newnham, R.M., Hazell, Z.J., Gehrels, M.J., Charman, D.J., Amesbury, M.J., 2018. Isochron-informed Bayesian age modelling for tephras and cryototephras: application to mid-Holocene Tuhua tephra, northern New Zealand. Book of Abstracts, Crossing New Frontiers: INTAV International Field Conference on Tephrochronology, "Tephra Hunt in Transylvania , pp. 95–96. https://iris.waikato.ac.nz/viewobject.html?cid=1&id=302685.

Lunina, O.V., Gladkov, A.S., 2016. Soft-sediment deformation structures induced by strong earthquakes in southern Siberia and their paleoseismic significance. Sedimentary Geology 344, 5–19. https://doi.org/10.1016/j.sedgeo.2016.02.014.

Manville, V., Wilson, C.J.N., 2004. The 26.5 ka Oruanui eruption, New Zealand: a review of the roles of volcanism and climate in the post-eruptive sedimentary response. New Zealand Journal of Geology and Geophysics 47, 525–547. https://doi.org/10.1080/00288306.2004.9515074.

Mastin, L.G., Carey, S.N., Van Eaton, A.R., Eychenne, J., Sparks, R.S.J., 2023. Understanding and modeling tephra transport: lessons learned from the 18 May 1980 eruption of Mount St. Helens. Bulletin of Volcanology 85, 1–21. https://doi.org/10.1007/s00445-022-01613-0.

Maurer, B.W., Green, R.A., Quigley, M.C., Bastin, S., 2015. Development of magnitude-bound relations for paleoliquefaction analyses: New Zealand case study. Engineering Geology 197, 253–266. https://doi.org/10.1016/j.enggeo.2015.08.023.

Mazumder, R., van Loon, A.J.T., Malviya, V.P., Arima, M., Ogawa, Y., 2016. Soft-sediment deformation structures in the Mio-Pliocene Misaki Formation within alternating deep-sea clays and volcanic ashes (Miura Peninsula, Japan). Sedimentary Geology 344, 323–335. https://doi.org/10.1016/j.sedgeo.2016.02.010.

McCraw, J.D., 2011. The wandering river: landforms and geological history of the Hamilton Basin. Geosciences Society of New Zealand, Wellington, Guidebook No. 16 (88p.).

McVerry, G.H., Zhao, J.X., Abrahamson, N.A., Somerville, P.G., 2006. Response spectral attenuation relations for crustal and subduction zone earthquakes. Bulletin of the New Zealand Society for Earthquake Engineering 39, 1–58. https://doi.org/10.5459/bnzsee.39.1.1-58.

Moebis, A., Cronin, S.J., Neall, V.E., Smith, I.E., 2011. Unravelling a complex volcanic history from fine-grained, intricate Holocene ash sequences at the Tongariro Volcanic Centre, New Zealand. Quaternary International 246, 352–363. https://doi.org/10.1016/j.quaint.2011.05.035.

Molenaar, A., Van Daele, M., Vandorpe, T., Degenhart, G., De Batist, M., Urrutia, R., Pino, M., Strasser, M., Moernaut, J., 2021. What controls the remobilization and deformation of surficial sediment by seismic shaking? Linking lacustrine slope stratigraphy to great earthquakes in South–Central Chile. Sedimentology 68, 2365–2396. https://doi.org/10.1111/sed.12856.

Montenat, C., Barrier, P., d'Estevou, P.O., Hibsch, C., 2007. Seismites: an attempt at critical analysis and classification. Sedimentary Geology 196, 5–30. https://doi.org/10.1016/j.sedgeo.2006.08.004.

Moon, V., de Lange, W., 2017. Final Report on EQC Potential Shallow Seismic Sources in the Hamilton Basin Project 16/717. University of Waikato.

Moretti, M., Ronchi, A., 2011. Liquefaction features interpreted as seismites in the Pleistocene fluvio-lacustrine deposits of the Neuquén Basin (Northern Patagonia). Sedimentary Geology 235, 200–209. https://doi.org/10.1016/j.sedgeo.2010.09.014.

Moretti, M., Sabato, L., 2007. Recognition of trigger mechanisms for soft-sediment deformation in the Pleistocene lacustrine deposits of the Sant'Arcangelo Basin (Southern Italy): seismic shock vs. overloading. Sedimentary Geology 196, 31–45. https://doi.org/10.1016/j.sedgeo.2006.05.012.

Moretti, M., van Loon, A.J.T., 2014. Restrictions to the application of 'diagnostic' criteria for recognizing ancient seismites. Journal of Palaeogeography 3, 162–173. https://doi.org/10.3724/SP.J.1261.2014.00050.

Moretti, M., Alfaro, P., Caselles, O., Canas, J.A., 1999. Modelling seismites with a digital shaking table. Tectonophysics 304, 369–383. https://doi.org/10.1016/S0040-1951(98)00289-3.

Morsilli, M., Bucci, M.G., Gliozzi, E., Lisco, S., Moretti, M., 2020. Sedimentary features influencing the occurrence and spatial variability of seismites (late Messinian, Gargano Promontory, southern Italy). Sedimentary Geology 401, 105628. https://doi.org/10.1016/j.sedgeo.2020.105628.

Nairn, I.A., 1980. Source, age, and eruptive mechanisms of Rotorua Ash. New Zealand Journal of Geology and Geophysics 23, 193–207. https://doi.org/10.1080/00288306.1980.10424206.

Newnham, R.M., Lowe, D.J., Green, J.D., 1989. Palynology, vegetation and climate of the Waikato lowlands, North Island, New Zealand, since c. 18,000 years ago. Journal of the Royal Society of New Zealand 19, 27–150. https://doi.org/10.1080/03036758.1989.10426443.

Newnham, R.M., Lowe, D.J., Williams, P.W., 1999. Quaternary environmental change in New Zealand: a review. Progress in Physical Geography 23, 567–610. http://ppg.sagepub.com/content/23/4/567.

Newnham, R.M., Eden, D.N., Lowe, D.J., Hendy, C.H., 2003. Rerewhakaaitu Tephra, a land-sea marker for the Last Termination in New Zealand, with implications for global climate change. Quaternary Science Reviews 22, 289–308. https://doi.org/10.1016/S0277-3791(02)00137-3.

Newnham, R.M., Lowe, D.J., Green, J.D., Turner, G.M., Harper, M.A., McGlone, M.S., Stout, S.L., Horie, S., Froggatt, P.C., 2004. A discontinuous ca. 80 ka record of late Quaternary environmental change from Lake Omapere, Northland, New Zealand. Palaeogeography, Palaeoclimatology, Palaeoecology 207, 165–198. https://doi.org/10.1016/j.palaeo.2004.02.007.

Nichols, R.J., 1995. The liquification and remobilization of sandy sediments. Geological Society, London, Special Publications 94, 63–76. https://doi.org/10.1144/GSL.SP.1995.094.01.06.

Obermeier, S.F., 1996. Use of liquefaction-induced features for paleoseismic analysis—an overview of how seismic liquefaction features can be distinguished from other features and how their regional distribution and properties of source sediment can be used to infer the location and strength of Holocene paleo-earthquakes. Engineering Geology 44, 1–76. https://doi.org/10.1016/S0013-7952(96)00040-3.

Okusa, S., 1985. Wave-induced stresses in unsaturated submarine sediments. Geotechnique 35, 517–532. https://doi.org/10.1680/geot.1985.35.4.517.

Owen, G., 2003. Load structures: gravity-driven sediment mobilization in the shallow subsurface. Geological Society, London, Special Publications 216, 21–34. https://doi.org/10.1144/GSL.SP.2003.216.01.03.

Owen, G., Moretti, M., 2011. Identifying triggers for liquefaction-induced soft-sediment deformation in sands. Sedimentary Geology 235, 141–147. https://doi.org/10.1016/j.sedgeo.2010.10.003.

Owen, G., Moretti, M., Alfaro, P., 2011. Recognising triggers for soft-sediment deformation: current understanding and future directions. Sedimentary Geology 235, 133–140. https://doi.org/10.1016/j.sedgeo.2010.12.010.

Ozcelik, M., 2016. Evaluation of soft sediment deformation structures along the Fethiye–Burdur Fault Zone, SW Turkey. Journal of Earth System Science 125, 343–358. https://doi.org/10.1007/s12040-016-0671-4.

Persaud, M., Villamor, P., Berryman, K.R., Ries, W., Cousins, J., Litchfield, N., Alloway, B.V., 2016. The Kerepehi Fault, Hauraki Rift, North Island, New Zealand: active fault characterisation and hazard. New Zealand Journal of Geology and Geophysics 59, 117–135. https://doi.org/10.1080/00288306.2015.1127826.

Peti, L., Hopkins, J.L., Augustinus, P.C., 2021. Revised tephrochronology for key tephras in the 130-ka Ōrākei Basin maar core, Auckland Volcanic Field, New Zealand: implications for the timing of climatic changes. New Zealand Journal of Geology and Geophysics 64, 235–249. https://doi.org/10.1080/00288306.2020.1867200.

Pidhorskyi, S., Morehead, M., Jones, Q., Spirou, G., Doretto, G., 2018. syGlass: interactive exploration of multidimensional images using virtual reality Head-mounted displays. arXiv https://doi.org/10.48550/arXiv.1804.08197 (preprint arXiv:1804.08197).

Pope, M.C., Fred Read, J., Bambach, R., Hofmann, H.J., 1997. Late Middle to Late Ordovician seismites of Kentucky, southwest Ohio and Virginia: sedimentary recorders of earthquakes in the Appalachian basin. Geological Society of America Bulletin 109, 489–503.

Rodríguez-Pascua, M.A., Calvo, J.P., De Vicente, G., Gómez-Gras, D., 2000. Soft-sediment deformation structures interpreted as seismites in lacustrine sediments of the Prebetic Zone, SE Spain, and their potential use as indicators of earthquake magnitudes during the Late Miocene. Sedimentary Geology 135, 117–135. https://doi.org/10.1016/S0037-0738(00)00067-1.

Rodríguez-Pascua, M.A., Silva, P.G., Perucha, M.A., Giner-Robles, J.L., Heras, C., Bastida, A.B., Carrasco, P., Roquero, E., Lario, J., Bardají, T., Pérez-López, R., Elez, J., 2016. Seismically induced liquefaction structures in La Magdalena archaeological site, the 4th century AD Roman Complutum (Madrid, Spain). Sedimentary Geology 344, 34–46. https://doi.org/10.1016/j.sedgeo.2016.01.025.

Rowley, J.R., Dahl, A.O., 1956. Modifications in design and use of the Livingstone piston sampler. Ecology 37, 849–851. https://doi.org/10.2307/1933080.

Schofield, J.C., 1965. The Hinuera Formation and associated Quaternary events (with an appendix on experimental alluviation). New Zealand Journal of Geology and Geophysics 8, 772–791.

Selby, M.J., Lowe, D.J., 1992. The middle Waikato Basin and hills. In: Soons, J.M., Selby, M.J. (Eds.), Landforms of New Zealand, Second edition Longman Paul, Auckland, pp. 233–255.

Sieh, K., Bursik, M., 1986. Most recent eruption of the Mono Craters, eastern central California. Journal of Geophysical Research - Solid Earth 91, 12539–12571. https://doi.org/10.1029/JB091iB12p12539.

Stirling, M., McVerry, G., Gerstenberger, M., Litchfield, N., Van Dissen, R., Berryman, K., Barnes, P., Wallace, L., Villamor, P., Langridge, R., 2012. National seismic hazard model for New Zealand: 2010 update. Bulletin of the Seismological Society of America 102, 1514–1542. https://doi.org/10.1785/0120110170.

Thomas, C.I., Ryan, M.A., Scholl, B., Guerrero-Given, D., Fitzpatrick, D., Kamasawa, N., 2021. Targeting functionally characterized synaptic architecture using inherent fiducials and 3D correlative microscopy. Microscopy and Microanalysis 27, 156–169. https://doi.org/10.1017/S1431927620024757.

Törő, B., Pratt, B.R., 2016. Sedimentary record of seismic events in the Eocene Green River Formation and its implications for regional tectonics on lake evolution (Bridger Basin, Wyoming). Sedimentary Geology 344, 175–204. https://doi.org/10.1016/j.sedgeo.2016.02.003.

Towhata, I., Taguchi, Y., Hayashida, T., Goto, S., Shintaku, Y., Hamada, Y., Aoyama, S., 2017. Liquefaction perspective of soil ageing. Géotechnique 67, 467–478. https://doi.org/10.1680/jgeot.15.P.046.

Tsuchida, H., 1970. Prediction and countermeasure against the liquefaction in sand deposits. Abstract of the Seminar in the Port and Harbor Research Institute, pp. 31–333.

Van Dissen, R.J., Seebeck, H., Litchfield, N., Barnes, P., Nicol, A., Langridge, R.M., Barrell, D., Villamor, P., Ellis, S., Rattenbury, M., Bannister, S., Gerstenberger, M., Ghisetti, F., 2021. Development of the New Zealand Community Fault Model – version 1.0. Proceedings of the 2021 New Zealand Society for Earthquake Engineering Annual Technical Conference, pp. 1–9.

Villamor, P., 2022. Paleoseismology of the newly discovered Te Puninga Fault, Hauraki Plains. EQC Project Number 20790 (Biennial Grants 2020) (GNS-EQC00036). Final Report BIG 012 2020, 31 December 2022. GNS Science, Lower Hutt.

Villamor, P., Almond, P., Tuttle, M.P., Giona-Bucci, M., Langridge, R.M., Clark, K., Ries, W., Bastin, S.H., Eger, A., Vandergoes, M., 2016. Liquefaction features produced by the 2010–2011 Canterbury earthquake sequence in southwest Christchurch, New Zealand, and preliminary assessment of paleoliquefaction features. Bulletin of the Seismological Society of America 106, 1747–1771. https://doi.org/10.1785/0120150223.

Walker, M., Johnsen, S., Rasmussen, S.O., Popp, T., Steffensen, J.-P., Gibbard, P., Hoek, W., Lowe, J.J., Andrews, J., Björck, S., Cwynar, L., Hughen, K., Kershaw, P., Kromer, B., Litt, T., Lowe, D.J., Nakagawa, T., Newnham, R.M., Schwander, J., 2009. Formal definition and dating of the GSSP (Global Stratotype Section and Point) for the base of the Holocene using the Greenland NGRIP ice core, and selected auxiliary records. Journal of Quaternary Science 24, 3–17. https://doi.org/10.1002/jqs.1227.

Walker, M., Head, M.J., Lowe, J., Berkelhammer, M., BjÖrck, S., Cheng, H., Cwynar, L.C., Fisher, D., Gkinis, V., Long, A., Newnham, R., Rasmussen, S.O., Weiss, H., 2019. Subdividing the Holocene Series/Epoch: formalization of stages/ages and subseries/subepochs, and designation of GSSPs and auxiliary stratotypes. Journal of Quaternary Science 34, 173–186. https://doi.org/10.1002/jqs.3097.

Watson, E.J., Swindles, G.T., Lawson, I.T., Savov, I.P., 2016. Do peatlands or lakes provide the most comprehensive distal tephra records? Quaternary Science Reviews 139, 110–128. https://doi.org/10.1016/j.quascirev.2016.03.011.

Wells, J.T., Prior, D.B., Coleman, J.M., 1980. Flowslides in muds on extremely low angle tidal flats, northeastern South America. Geology 8, 272–275.

White, J.D.L., Houghton, B.F., 2006. Primary volcaniclastic rocks. Geology 34, 677–680. https://doi.org/10.1130/G22346.1.

Williams, P.W., 2021. Quaternary uplift and fault movement near Waitomo, North Island, New Zealand. New Zealand Journal of Geology and Geophysics, 1–11 https://doi.org/10.1080/00288306.2021.1996401.

Wolff-Boenisch, D., Gislason, S.R., Oelkers, E.H., Putnis, C.V., 2004. The dissolution rates of natural glasses as a function of their composition at pH 4 and 10.6, and temperatures from 25 to 74 C. Geochimica et Cosmochimica Acta 68, 4843–4858. https://doi.org/10.1016/j.gca.2004.05.027.

Wood, F.M., Yamamuro, J.A., Lade, P.V., 2008. Effect of depositional method on the undrained response of silty sand. Canadian Geotechnical Journal 45, 1525–1537. https://doi.org/10.1139/T08-079.

Yang, Q., Bursik, M., Pouget, S., 2019. Stratigraphic and sedimentologic framework for tephras in the Wilson Creek Formation, Mono Basin, California, USA. Journal of Volcanology and Geothermal Research 374, 197–225. https://doi.org/10.1016/j.jvolgeores.2019.02.007.

Youd, T.L., 1991. Mapping of earthquake-induced liquefaction for seismic zonation. Proceedings of the Fourth International Conference on Seismic Zonation pp. 111–147.

Zhou, Y.-G., Xia, P., Ling, D.-S., Chen, Y.-M., 2020. Liquefaction case studies of gravelly soils during the 2008 Wenchuan earthquake. Engineering Geology 274, 105691. https://doi.org/10.1016/j.enggeo.2020.105691.

Supplementary material

Supplementary tables

Table S1. Detailed information of lake cores.

Lake	Composite core depth[1]	Overlapping cores		Tephras classified[3]							Notes[4]
Name (label)	(mbl)	Label[2]	(mbl)	Tu	Ma	Op	Mm	Wh	Rr	Rk	
Ngāroto (S1)	0.05–4.30	S1-A-1	0.02–2.35		i	d	i		i	i	1
		S1-A-2	1.84–4.20						ds		
		S1-A-3	0.05–1.91	d	d	d	i				
		S1-A-4	2.04–4.15								
Mangakaware (S2)	0.00–3.19	S2-A-1	0.00–3.18	d	i	i	i	i	i	i	2
		S2-A-2	0.00–1.86		i	i	i	i	i	i	
		S2-B-1	0.00–0.84	i	i						
Maratoto (S3)	0.00–3.80	S3-A-1	0.00–3.80	i	ds	i	i	i	i	i	2, 3
		S3-A-2	0.00–3.10	d	i	i	i	i	i	i	
		S3-A-3	0.10–2.80	d	d	d	i	ds	i	i	
		S3-B-1	0.00–1.40						i	i	
		S3-B-2	0.00–1.40						i	i	
		S3-C-1	0.00–3.15	d	i	i		i	i	i	
		S3-C-2	0.00–1.75	i	i	i	i	i	i		
		S3-C-3	0.00–1.63	i	i	i	d	ds	i	d	
		S3-D-1	0.00–2.39	i	i	i	i	i	i	i	
		S3-E-1	0.00–1.93	i	i	i		i	i	i	
		S3-F-1	0.00–1.70	d	i	i	i	i	i		
		S3-G-1	0.00–1.83	d	i	i		i	i		
		S3-G-2	0.00–2.40	i	ds	i		i	i	i	
		S3-G-3	0.50–2.67	i	i	i	i	i	i	i	
		S3-H-1	0.00–3.12		i	d	i	i	i	d	
		S3-H-1	0.00–2.64	i	i	d		d	i		
		S3-H-1	0.00–2.17	i	d	i		i	i	i	
		S3-I-1	0.75–2.96	i	i	i		i	i	i	
		S3-J-1	0.50–1.93		i	d			i		
		S3-J-2	0.50–2.82	i	i	i	i	i	i	i	
		S3-K-1	0.00–2.03	i	i	i	i	i	i	d	
		S3-L-1	0.00–2.60	i	ds	i		ds		i	
Rotoroa (C1)	0.11–3.06	C1-A-1	0.11–1.67	i	i	i					4
		C1-A-2	1.26–3.46	i	i	i	i	i	i	i	
	0.00–3.17	C1-B-1	0.00–1.72	i							5
		C1-B-2	1.00–2.15	i	i	i	i	i	ds		
	1.00–3.03	C1-C-1	1.00–2.25					i	ds		
		C1-C-2	1.40–3.03						ds		
	0.00–3.35	C1-D-1	0.00–1.77	i	i	i	i				
		C1-D-2	1.50–3.93	i	i	i	i	i	ds	i	
	0.00–1.76	C1-E-1	0.00–1.75	i	i	ds	d	ds	ds		
	0.00–1.83	C1-F-1	0.00–1.17	i	i	i	i	i			
		C1-F-2	0.10–1.76	i	ds		d	i	ds	i	
	0.00–3.98	C1-G-1	0.00–2.21	i	i	i	i				
		C1-G-2	2.00–4.08			i	i	ds	ds	i	

Table S1. *(continued)*

Lake	Composite core depth[1]	Overlapping cores		Tephras classified[3]							Notes[4]
Name (label)	(mbl)	Label[2]	(mbl)	Tu	Ma	Op	Mm	Wh	Rr	Rk	
Rotokaeo (C2)	0.10–4.04	C2-A-1	0.10–1.56	i	i						4
		C2-A-2	1.00–3.24	ds	ds	i	ds	ds	d		
		C2-A-3	2.50–4.65			i	i	i	ds	ds	
Waiwhakareke (C3)	0.13–4.37	C3-A-1	0.13–1.87	i	i	i					4
		C3-A-2	1.00–3.16	i	i	ds	d	i	i		
		C3-A-3	2.50–4.75	i	d		i	i	i	i	
Rotokauri (C4)	0.03–6.94	C4-A-1	0.03–2.04	ds	d						1
		C4-A-2	1.95–4.10	ds	i	i	i	d			
		C4-A-3	3.53–6.71					d	ds	i	
		C4-A-4	0.58–3.70	i	i	i	i	d			
		C4-A-5	3.55–5.95					i	ds	i	
Kainui (N1)	0.05–4.02	N1-A-1	0.00–2.10	i	i	i		i	ds	i	2
		N1-A-2	0.00–2.90	i	i	i		i	ds	i	
		N1-B-1	0.05–1.88								1
		N1-B-2	1.54–4.14	i	i	i	i	i	ds	ds	
		N1-B-3	0.07–3.17	i	i	i	i	d	d		
		N1-B-4	1.04–3.41	i	i	i	i	i	d		
Rotokaraka (N2)	1.00–6.57	N2-A-1	1.00–3.65	i		d		ds	ds		2
		N2-A-2	2.00–4.36		d	d		i	ds	i	
		N2-A-3	4.00–5.74						ds	i	
		N2-A-4	3.00–4.95					i	ds	i	
Leeson's Pond (N3)	1.51–4.56	N3-A-1	3.00–5.70	i				ds	ds	i	2
		N3-A-2	3.00–5.30	i		i		ds	ds	i	
		N3-A-3	1.50–2.70	i	d	i					

mbl–metre below lake bed; Tu = Tuhua tephra; Ma = Mamaku tephra; Op = Opepe tephra; Mm = Mangamate tephra; Wh = Waiohau tephra; Rr = Rotorua tephra; Rk = Rerewhakaaitu tephra

[1]Composite cores were created from information of one or more overlapping cores; an example for Lake Rotokaeo (C2) is provided in supplementary Fig. S1.

[2]The letters A to L (forming the middle part of the core labels) represent different coring locations within the central part of a lake, whereas the last digit in the label denotes a core taken at a specific coring location. Note that the core labels for Maratoto (S3) were changed from those used in the original publication to align with the nomenclature used for later coring as follows (old labels in brackets follow Green and Lowe (1985) and unpublished core logs): S3-A-1 (4,1a), S3-A-2 (4,1b), S3-A-3 (4,1d), S3-B-1 (4,1h), S3-B-2 (4,1i), S3-C-1 (5,1a), S3-C-2 (5,1b), S3-C-3 (5,1c), S3-D-1 (6,1a), S3-E-1 (7,1a), S3-F-1 (1Nb), S3-G-1 (5Wb), S3-G-2 (5Wc), S3-G-3 (5Wa), S3-H-1 (5Ec), S3-H-2 (5Eb), S3-H-3 (5Ea), S3-I-1 (6Wa), S3-J-1 (6Eb), S3-J-2 (6Ea), S3-K-1 (7Wa), S3-L-1 (7Ea).

[3]Tephra layers were classified as "soft-sediment deformation structures present" (ds), "intact" (i), and "discontinuous" (d). Cells that were left empty denote that the respective tephra layers were not cored or identified in the sediment core. Examples of classified tephra layers are provided in supplementary Fig. S2.

[4]Notes: (1) cored in 2016; (2) published by Lowe (Lowe 1988); (3) published Green and Lowe (1985); (4) cored in 2020; (5) cored in 2022.

Table S2. Sampling list of lake cores.

Lake	Overlapping cores		Sampling		
Name (label)	Label[2]	(mbl)	Depth	Stratigraphy	Type
Ngāroto (S1)	S1-A-1	0.02–2.35	1.12	Ma	gs
			1.91	Rr	gs
			2.05	Rk	gs
	S1-A-2	1.84–4.20	1.85	Rr*	gs
Rotoroa (C1)	C1-A-1	0.11–1.67	1.30	Lake sediment	al
			1.37	Tu	gs
			1.42	Ma	gs
	C1-A-2	1.26–3.46	2.06	Tu	gs
			2.14	Ma	gs
			2.79	Lake sediment	al
			2.91	Wh	gs
			3.11	Rr	gs
			3.31	Rk	gs
Rotokaeo (C2)	C2-A-1	0.10–1.56	1.53	Tu	gs
			1.59	Ma	gs
			1.68	Lake sediment	al
	C2-A-2	1.00–3.24	1.46	Tu	gs
			1.54	Ma	gs
			2.92	Lake sediment	al
			3.12	Rr	gs
	C2-A-3	2.50–4.65	2.53	Tu	gs
			3.53	Rr	gs
			3.83	Rk	gs
			3.89	Lake sediment	al
Waiwhakareke (C3)	C3-A-1	0.13–1.87	1.38	Tu	gs, bd
			1.44	Ma	gs
			1.50	Lake sediment	al
	C3-A-2	1.00–3.16	1.67	Lake sediment	bd
			1.89	Tu*	gs
			1.97	Ma*	gs
			2.09	Lake sediment	bd
			2.75	Wh*	gs
			3.06	Lake sediment	al
	C3-A-3	2.50–4.75	3.21	Wh	gs
			3.40	Lake sediment	bd
			3.62	Rr*	gs, bd
			3.90	Lake sediment	bd
			4.17	Lake sediment	al
			4.23	Rk*	gs

Table S2. *(continued)*

Lake	Overlapping cores depth		Sampling		
Name (label)	Label[1]	(mbl)	Depth	Stratigraphy[2]	Type[3]
Rotokauri (C4)	C4-A-1	0.03–2.04	1.75	Lake sediment	bd
			1.92	Tu*	gs
			2.12	Tu*	gs
	C4-A-2	1.95–4.10	2.07	Lake sediment	oc
			2.20	Ma	gs
			2.46	Lake sediment	bd
	C4-A-3	3.53–6.71	3.93	Lake sediment	oc
			3.98	Rr	gs
			4.03	Lake sediment	oc
	C4-A-4	0.58–3.70	1.68	Lake sediment	oc
			1.74	Tu	gs
			1.87	Lake sediment	oc
	C4-A-5	3.55–5.95	3.72	Wh	gs
			4.03	Rr*	gs
			4.42	Rk	gs
Kainui (N1)	N1-B-2	1.54–4.14	2.08	Tu	gs
			2.16	Ma	gs
			2.96	Wh	gs
			3.08	Lake sediment	bd
			3.21	Rr*	gs
			3.43	Lake sediment	bd
	N1-B-3	0.07–3.17	2.08	Tu	gs
			2.15	Ma	gs
	N1-B-4	1.04–3.41	2.29	Tu	gs
			2.42	Ma	gs
			3.22	Wh	gs

[1]See description to supplementary Tab. S1.

[2]Sampling was performed on lake sediment or on specific intact tephra layers (Tu = Tuhua tephra; Ma = Mamaku tephra; Op = Opepe tephra; Mm = Mangamate tephra; Wh = Waiohau tephra; Rr = Rotorua tephra; Rk = Rerewhakaaitu tephra). The asterisk indicates that sampling was performed on liquefied tephra layers.

[3]Differerent types of samples were taken: al = Atterberg limits; bd = Bulk density; gs = Grain size; oc = Organic content. See description in the Methods section for further details.

Supplementary figures

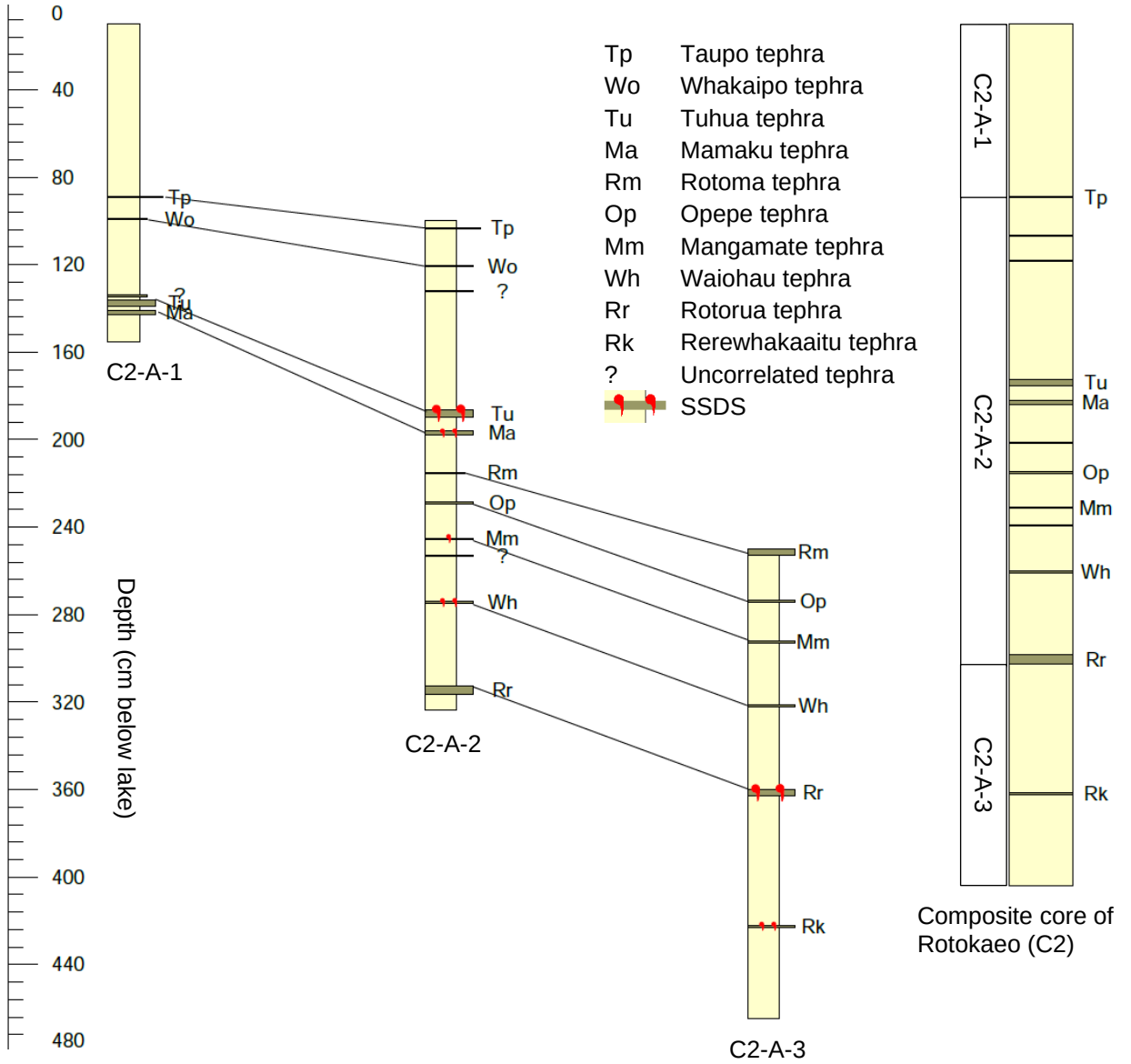

Fig. S1. Example for construction of composite core at Lake Rotokaeo (C2). The composite core was created by stacking three overlapping cores (i.e., C2-A-1, C2-A-2, C2-A-3), being well-correlated (connected from one to another) based on distinctive tephra layers present in the cores in different superpositions. The tephra layers are not located at exactly the same absolute core depths mainly because of local variability in the lake sediments. This variability resulted in depth offsets for some tephra layers. The depth scale of cores was kept constant.

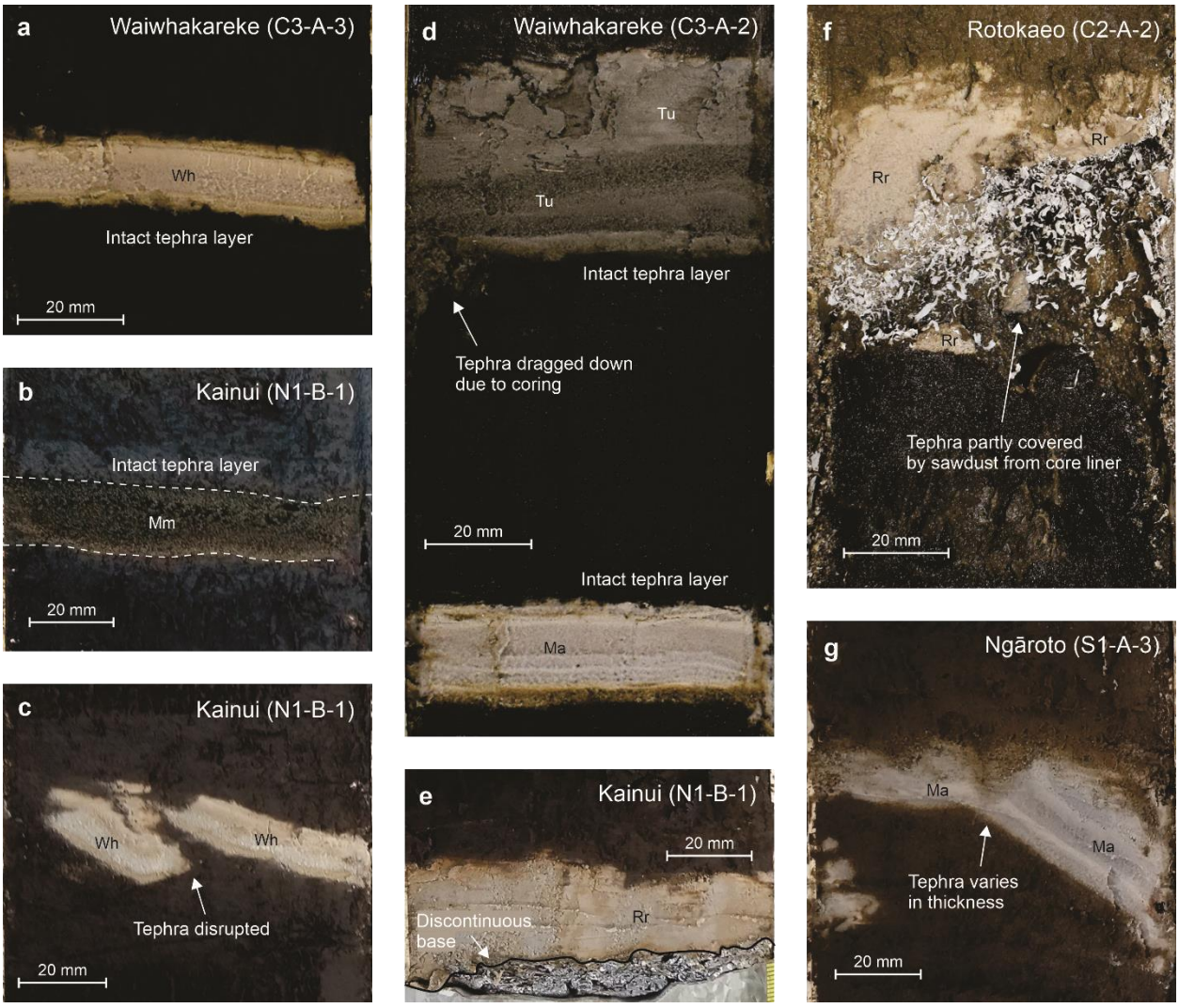

Fig. S2. Examples of tephra layers intercalated in lake sediment. (a-b, d) Tephra layers being classified as "intact". Small artefacts due to the coring process may be present (i.e., a tephra is dragged down along the coring barrel). (c, e-g) Tephra layers being classified as "discontinuous". Tephras were either disrupted (c), exhibited a discontinuous base (e), were not entirely exposed (f), or significantly varied in thickness (g).

References

Green JD and Lowe DJ (1985) Stratigraphy and development of c. 17 000 year old Lake Maratoto, North Island, New Zealand, with some inferences about postglacial climatic change. New Zealand Journal of Geology and Geophysics 28(4): 675-699. https://doi.org/10.1080/00288306.1985.10422541

Lowe DJ (1988) Late Quaternary volcanism in New Zealand: towards an integrated record using distal airfall tephras in lakes and bogs. Journal of Quaternary science 3(2): 111-120. https://doi.org/10.1002/jqs.3390030202